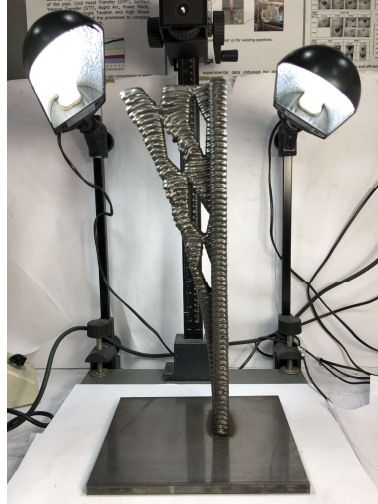




TÉCNICO
LISBOA



Development of Wire Arc Additive Manufacturing (WAAM) procedures that allow depositing very complex structures without support

Luís Manuel Guilhoto Marques Fialho

Thesis to obtain the Master of Science Degree in

Mechanical Engineering

Supervisors: Prof. Inês da Fonseca Pestana Ascenso Pires
Prof. Eurico Gonçalves Assunção

Examination Committee

Chairperson: Prof. Rui Manuel dos Santos Oliveira Baptista
Supervisor: Prof. Eurico Gonçalves Assunção
Member of the Committee: Prof. Carlos Manuel Alves de Silva

June 2019

To my family

Acknowledgments

I would like to express my sincere gratitude to Professor Eurico Assunção and to Professor Inês Pires and to Doctor Filomeno Martina for the opportunity given.

I am also most grateful to all members of the Welding Engineering and Laser Processing Centre in Cranfield University for all the help and guidance.

To my colleagues and dearest friends who always showed their support and companionship, in particular, to Tiago Oliveira, Duarte Tamen, João Ramalho, Francisco Monteiro, Francisco Vaz, Francisco Vieira, Jorge Milhomem and João Miguel Costa for their help and support in so many different ways along this journey.

Finally, my deepest gratitude to my parents and my brother, who made possible this accomplishment. Without them I would be nothing.

Resumo

Wire + Arc Additive Manufacturing (WAAM) é um processo de fabrico aditivo que tem alcançado um elevado interesse nos últimos anos e que tem sido considerado como parte integrante da quarta revolução industrial uma vez que reduz mão-de-obra especializada, desperdício, tempo e custo quando comparado com os métodos convencionais.

No presente trabalho, uma parte representativa de uma peça que apresenta uma altura de 5 metros foi produzida recorrendo ao WAAM. O material utilizado foi um fio de aço carbono ER70S-6 que foi depositado utilizando um processo de CMT. Um software beta de WAAM desenvolvido pela Universidade de Cranfield foi aplicado e o seu contributo para a deposição no caso de Free Forming AM foi validado, gerando as trajetórias de deposição. Após um extenso processo de ensaios/testes, a peça representativa final foi depositada. A microestrutura, a macroestrutura, a porosidade, a micro-dureza, a eficiência da trajetória de deposição e a deformação do substrato foram analisadas e comparadas. A microestrutura e a macroestrutura, bem como a porosidade, apresentaram-se concordantes com a literatura. A correlação entre a dureza de Vickers e a tensão de rotura bem como com a tensão de cedência traduziam-se numa peça final com um valor de 823.27 MPa e de 465.64 MPa , respetivamente. Os valores encontram-se em sintonia com os que seriam de esperar para o mesmo material mas fabricado através de métodos convencionais. Adicionalmente, foram propostos novos métodos de melhoria relativamente à eficiência da trajetória de deposição e à mitigação de deformações do substrato.

Em suma, este trabalho demonstrou que é possível depositar uma peça vertical, que apresenta uniões complexas, cujas secções sejam de dimensões reduzidas utilizando o WAAM.

Palavras-chave: wire + arc additive manufacturing, software para WAAM, aço carbono, CMT, forma livre

Abstract

Wire + Arc Additive Manufacturing (WAAM) is an additive manufacturing process that has received an increasingly interest in recent years and is being catalogued as being part of the 4th industrial revolution since it reduces specialized labour, waste, time and cost when compared to conventional methods.

In this work a representative complex structure from a 5 meters height part was produced using WAAM. The material used was an ER70S-6 mild steel wire and a CMT process was employed. A beta WAAM software developed by Cranfield University was used and its application in Free Forming AM was validated in this work, generating the deposition paths. After a considerable amount of trials, a final part was deposited. Microstructure, macrostructure, porosity, microhardness, path efficiency and substrate deformation were studied and compared. Microstructure and macrostruture were in agreement with the literature as well as porosity. The correlation between vickers hardness and UTS and YS resulted in a final part with a mean value of UTS of 823.27 *MPa* and of YS of 465.64 *MPa* which are in the range expected for mild steel. Additionally path efficiency and substrate deformations improving techniques were proposed.

With respect to this work, it is shown that building a part that possesses complex intersections that need a type of free form deposition, in an upwards direction is achievable using WAAM.

Keywords: wire + arc additive manufacturing, WAAM Software, mild steel, CMT, free form

Contents

Acknowledgments	v
Resumo	vii
Abstract	ix
List of Tables	xiii
List of Figures	xv
Nomenclature	xix
Glossary	xxi
1 Introduction	1
1.1 Motivation	1
1.2 State of the Art	2
1.3 Objectives	4
1.4 Thesis Outline	6
2 Background	7
2.1 Additive Manufacturing	7
2.2 Wire and Arc Additive Manufacturing	9
2.3 Wire and Arc Additive Manufacturing Processes	10
2.3.1 Gas Tungsten Arc Welding	11
2.3.2 Plasma Arc Welding	11
2.3.3 Gas Metal Arc Welding	11
3 Materials and Methodology	15
3.1 Methodology	15
3.2 Materials	16
3.3 Equipment Set-up	16
3.4 Deposition Parameters	19
3.5 Deposition of the Part	21
3.6 Path Generator	22
3.7 Samples Preparation	26
3.7.1 Sample Study Region	26
3.7.2 Samples Preparation Methodology	29

3.8	Macro and Microscopy Observation	30
3.9	Hardness Test	31
3.10	Path Efficiency and Substrate Deformation	32
4	Results and Analysis	35
4.1	Deposition Parameters	35
4.1.1	First Stage	35
4.1.2	Second Stage	38
4.1.3	Third Stage	38
4.1.4	Fourth Stage	43
4.2	Final Part	47
4.3	Optical Macro and Microscopy Analysis	51
4.3.1	Optical Macroscopic Observation	52
4.3.2	Optical Microscopic Observation	53
4.3.3	Conclusion Remarks	59
4.4	Micro Hardness	60
4.5	Path Efficiency	61
4.6	Substrate Deformation	63
5	Conclusions	65
5.1	Achievements	65
5.2	Future Work	66
	Bibliography	67
A	Technical Data Sheets	71
B	Software Files	73
B.1	Builddata File	74
B.2	ABB Programme File	75

List of Tables

- 1.1 Summary of the best process conditions [4] 3

- 2.1 Technological and Economic Opportunities and Limitations of AM [9] 8
- 2.2 Comparison between Powder AM and Wire AM [11] 9
- 2.3 Effect of changes in process variables on weld attributes [24] 12

- 3.1 Chemical composition of the substrate and of the deposited part 16

- 4.1 Parameters used in the first stage of the experiments 37
- 4.2 Dimensions of the experiments of the first stage 37
- 4.3 Parameters applied in the second stage of the experiments 38
- 4.4 First experiment parameters of third stage 39
- 4.5 Second experiment parameters of third stage 40
- 4.6 Third experiment parameters of third stage 41
- 4.7 Fourth experiment parameters of third stage 41
- 4.8 Experiments comparison 42
- 4.9 Final part parameters 48
- 4.10 Comparison between actual layer height and expected layer height 50
- 4.11 Correlation of Vickers Hardness with Ultimate Tensile Strength and Yield Strength 60
- 4.12 Duration of deposition and path efficiency 62

List of Figures

- 1.1 Stainless steel free-form continuous deposition [2] 2
- 1.2 Deposited samples [3] 3
- 1.3 WAAM system architecture [5] 4
- 1.4 CAD Model of the part to be achieved 5

- 2.1 Geometric Complexity vs Quantity for metal prudctions methods [8] 7
- 2.2 Current main AM processes [10] 8
- 2.3 Schematic diagram of the processes - (a) GMAW, (b) GTAW and (c) PAW [11] 10
- 2.4 High-speed images of a CMT droplet transfer [26] 13
- 2.5 Current and Voltage waveforms of a CMT process [26] 13

- 3.1 Methodology [17] 15
- 3.2 Semi-automatic horizontal bandsaw Bomar Individual 610.440GH 16
- 3.3 First Set-Up 17
- 3.4 Second Set-Up 18
- 3.5 Experiment performed for the largest section 19
- 3.6 Experiment performed for the smallest section 20
- 3.7 Experiments performed to obtain the intersections 21
- 3.8 (a) RS Pro Digital Thermometer 206 - 3722, (b) Digital Calliper SPI 12-527-8 22
- 3.9 Rhinoceros software interface 23
- 3.10 Representation of the layers in Rhinoceros 23
- 3.11 Grasshopper software interface 24
- 3.12 Startrite 316 27
- 3.13 Final part cutting process 27
- 3.14 Struers Discotom - 60 28
- 3.15 Regions of interest of the final part 28
- 3.16 ATA Saphir 520 29
- 3.17 Washing workstation (a) Water washing workstation (b) Alcohol washing workstation . . 30
- 3.18 MetPrep sample drying station 30
- 3.19 Nikon Optishot microscope 31
- 3.20 Schott KL 1500 electronic 31

3.21	Hardness test set-up and equipment (a) Hardness test set-up (b) Zwick Roell ZHV	32
3.22	Software for the calculation of micro hardness	32
4.1	Dimensions of the base of the final part	36
4.2	Experiments performed for the parametrization of the base of the final part	36
4.3	Third stage - First experiment	39
4.4	Third stage - Second experiment	40
4.5	Third stage - Third experiment	40
4.6	Third stage - Fourth experiment	41
4.7	Experiments comparison graph	42
4.8	CAD comparison between the part to be achieved and the part actually deposited (a) Part to be achieved (b) Final part	43
4.9	Fourth stage - First experiment	44
4.10	Fourth stage - Second experiment	44
4.11	Angle of closure of second experiment	45
4.12	Fourth stage - Third experiment	45
4.13	Angle of closure of third experiment	45
4.14	Fourth stage - Fourth experiment	46
4.15	Angle of closure of fourth experiment	46
4.16	Fourth Stage - Fifth experiment	47
4.17	Angle of closure of fifth experiment	47
4.18	Final part	48
4.19	Number of Layers vs % of Deviation - Set Layer	49
4.20	Defects of the final part	51
4.21	Macro-structure of the final part and of the second experiment of the third stage	52
4.22	Substrate sample of third stage - Second experiment	54
4.23	Wall sample of third stage - Second experiment	54
4.24	Final part sample of substrate	55
4.25	Final part sample of base	55
4.26	Final part sample of first intersection	56
4.27	Final part sample of second intersection	57
4.28	Final part sample of third intersection	57
4.29	Final part sample of fourth intersection	58
4.30	Final part sample of porosity region	58
4.31	Final part sample of middle section	59
4.32	Correlation of Vickers Hardness with Ultimate Tensile Strength and Yield Strength	61
4.33	Path efficiency	62
4.34	Substrate usage during experiments	63
A.1	Deposited material data sheet	72

B.1	Builddata example file	74
B.2	ABB programme example file	75

Nomenclature

HV Vickers hardness.

OT On time.

PE Path efficiency.

TS Tensile strength.

TT Total time.

YS Yield strength.

Glossary

AM	Additive Manufacturing
ASTM	American Society for Testing and Materials
CAD	Computer-Aided Design
CMT Adv. pol.	Cold Metal Transfer Advanced polarity
CMT Cont.	Cold Metal Transfer continuous trajectory
CMT	Cold Metal Transfer
CNC	Computer Numerical Control
CTWD	Contact Tip to Work Distance
DLF	Direct Laser Fabrication
EBF	Electron Beam Freeform Fabrication
EBM	Electron Beam Melting
GMAW	Gas Metal Arc Welding
GTAW	Gas Tungsten Arc Welding
HAZ	Heat Affected Zone
IC	Initial Current
IV	Initial Voltage
LEV	Local Exhaust Ventilation
MAG	Metal Active Gas
MIG	Metal Inert Gas
PAW	Plasma Arc Welding
SEM	Scanning Electron Microscopy
SGB	Solidification Grain Boundaries
SLS Cont.	Selective Laser Melting
TIG	Tungsten Inert Gas
TS	Travel Speed
UTS	Ultimate Tensile Strength
WAAM	Wire + Arc Additive Manufacturing
WFS	Wire Feed Speed
WLAM	Wire and Laser Additive Manufacturing
YS	Yield Strength

Chapter 1

Introduction

1.1 Motivation

As the environment is a constant concern nowadays, industry, in a response to both economic pressures and the need for sustainable developments, imposed by governments, has been forced to find alternative manufacturing technologies to conventional ones in order to reduce quantity of raw material wasted during manufacture. Thus, with increasing adherence, emerged in 1987 in response to these guidelines the Additive Manufacturing (AM) process. Initially used as a rapid prototyping process, it has been slowly replacing some conventional techniques since this process reduces specialized labour, waste, time and cost.

Being a more economical and more sustainable process, it uses a smaller amount of raw material and has shorter production times. Additive manufacturing is still characterized by allowing greater freedom in the design phase as a consequence of the ease of production of more complex geometries, which strengthens weight reductions in the component, as well as facilitating the assembly of assemblies formed by several subsets.

Additive Manufacturing has become the subject of a substantial amount of research, leading to improvements on the product designs, material, process engineering, simulation software and data transfer. The recent developments focus in the production of metallic components regarding complex shapes. An emphasis on welding technologies using arc sources and wire feed is being performed. The key advantages of wire and arc additive manufacturing are: high deposition rate, reduced costs and the easy access to the process.

Considering the aforementioned and that AM is being catalogued as part of the 4th industrial revolution it can be stated that Wire + Arc Additive Manufacturing is an important process for the near future bringing humans one step closer to solving the problem of waste material in the worldwide manufacture industry. It is, therefore, important that continuous research of WAAM moves forward in order to become globally relevant. That is why there is a clear interest in being part of this development.

1.2 State of the Art

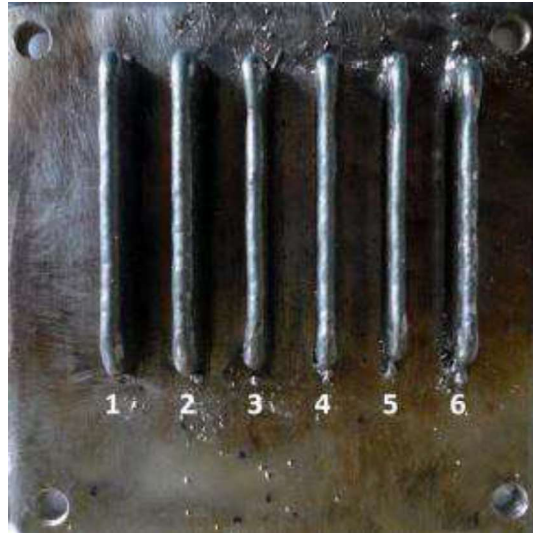
Previous works that contributed for the development and achievement of the pretended objectives will be highlighted in this section 1.2.

The type of deposition of thin structures built upwards is a novelty, therefore there is not much work performed with these characteristics. For example, thin walls were already achieved in diverse works. Cong et al. [1] studied thin walls with aluminium as opposed to other authors that will be mentioned in the following paragraphs and section which reach the same outcome for steel and titanium. Yet, small structures were not achieved with an acceptable outcome. Gou [2] performed a continuous metal free-form deposited structure with aluminium and stainless steel. In this case an efficient active cooling system was necessary. In the present work a free-form type of deposition was employed, however a complex active cooling system was not applied because the dimension of the structures did not required so. On the other hand it was perceived that the interlayer temperature is a critic variable in order to achieve a sound part. In figure 1.1 are displayed the free-forms structures.

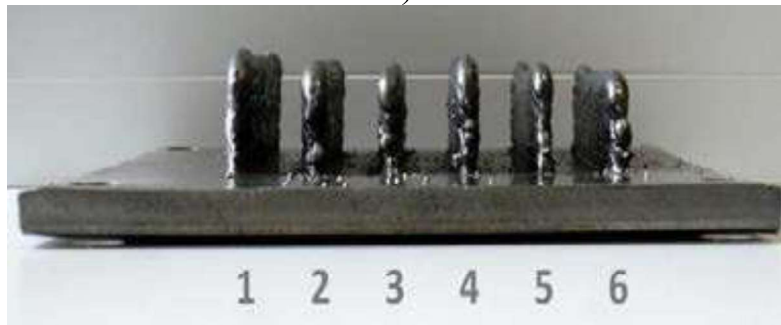


Figure 1.1: Stainless steel free-form continuous deposition [2]

Liberini et al. [3] performed a study of optimal parameters in WAAM for an ER70S-6 steel. Six samples, each with fifteen layers, were deposited. The characterization of the samples consisted in: macrographic observations, micrographic analysis by SEM, vickers microhardness and surface analysis by confocal microscopy. The parameters were acquired and compared. The main conclusion is that small alteration of the process parameters do not produce changes on the deposition since the cooling curve is the variable that contributes the most to the micro structure characterization. The latter is not affected by the process parameters. Figure 1.2 shows the samples tested.



a)



b)

Figure 1.2: Deposited samples [3]

Still regarding optimum process conditions, Prado-Cerqueira et al. [4] performed an analysis of process conditions for the deposition of mild-steel thin-walls in WAAM. A ER70S-6 mild steel 0.8 mm diameter wire was deposited using various MIG and CMT processes. The shielding gas used was a mixture of CO₂ (15%) and Argon (85%). Evaluation of hardness profiles were performed and it was concluded that the best process to use is simple CMT and that there is "an important lack of information about the influence of the microstructure in the behaviour of parts obtained by additive manufacturing process in general, and in WAAM in particular". In the next table 1.1 is presented the summary of the best process conditions.

Sample nº	Process	Most Homogeneous Hardness Profiles (Figure 6a–g)	Highest Values of Mean Hardness (Figure 6h)	Best Estimated UTS [55] (Table 5)	Absence of Decohesiated Layer at the Surface (Figure A2)
1	MIG	X	X		
2	CMT	X		X	X
3	CMT Adv pol. 0				X
4	CMT Adv pol. 0				X
5	CMT Adv pol. -5				X
6	CMT Adv pol. +5				X
7	CMT Cont.	X		X	X

Table 1.1: Summary of the best process conditions [4]

Busachi et al. [5] designed a WAAM based manufacturing system. In his work proposed a WAAM system architecture shown in the following figure 1.3.

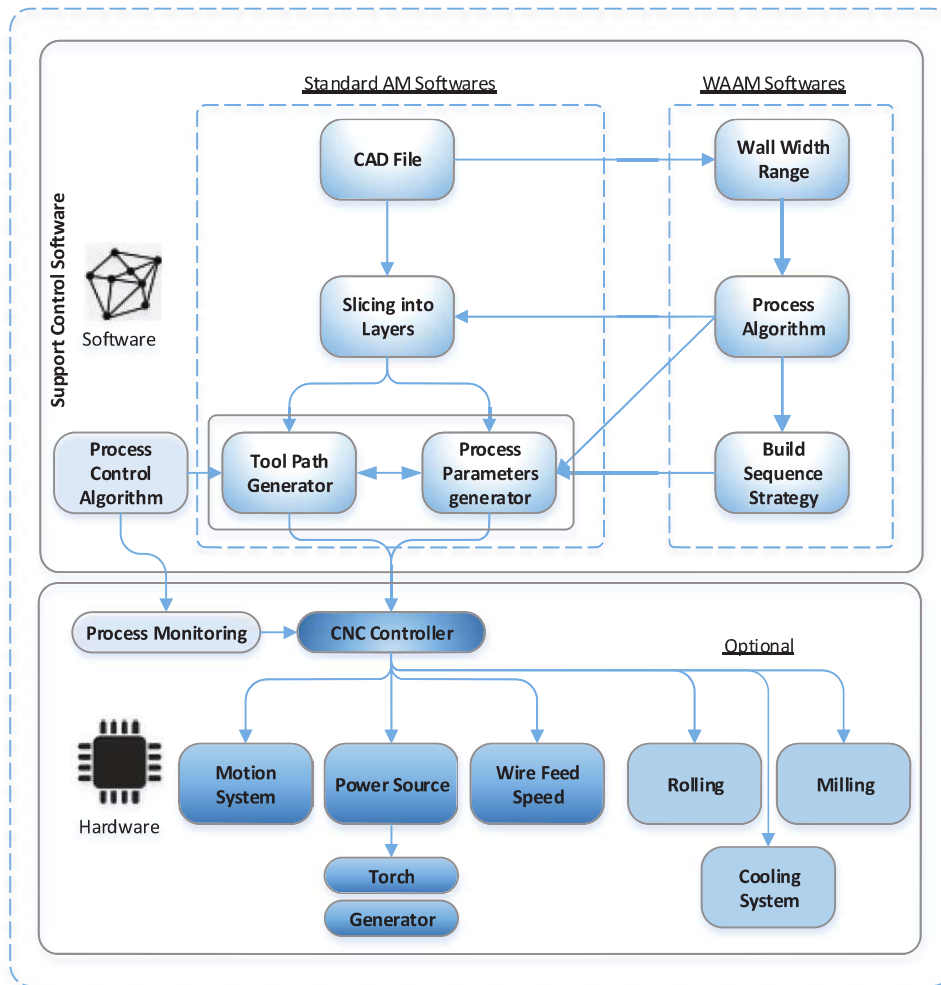


Figure 1.3: WAAM system architecture [5]

This architecture is composed by a hardware and a software module. The files produced by the software need to be in a format that the hardware modules are able to understand in order to allow the WAAM software to be fully automated.

An advanced WAAM software developed by Cranfield University is currently in its Beta version. The software receives a CAD model and with some variables that the user inputs, produces files to be read by the robot. The ultimate goal is to deposited parts completely in a autonomous form.

1.3 Objectives

The main objective of this work is to achieve a deposition strategy that is able to deposit the structure represented in the following figure 1.4.

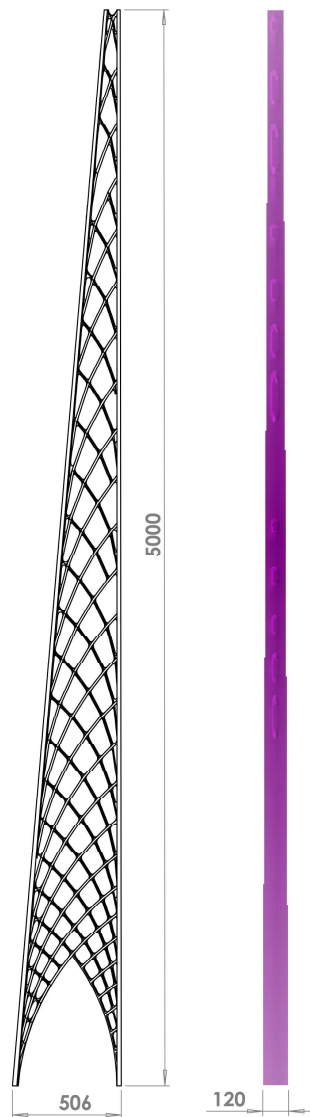


Figure 1.4: CAD Model of the part to be achieved

The part should meet the following requirements:

- Near net-shape dimensions
- No macro-structural defects
- No micro-structural defects
- Benchmark mechanical properties

The targets required to accomplish such requirements are:

- Building the part with a Mild Steel wire using Cold Metal Transfer (CMT) as a welding method
- Employing the Cranfield software for the generation of the path, contributing to its development

- Working out the best parameters and employ them in the deposition
- Depositing and analysing the part to be achieved.

1.4 Thesis Outline

This work is divided into five main chapters:

1. - Introduction - In this chapter the main objectives are enumerated. Also the state of the art is outlined. In the latter are reported previous works that contributed to a better understanding and development of this actual work.
2. - Background - Provides a valuable overview of the topics that play an important role thorough this work.
3. - Materials and Methodology - In this chapter, materials are classified and identified. Also the methodologies used to collect the required data are addressed.
4. - Results and Analysis - Collected data is analysed and results are presented in a particular and in a general point of view.
5. - Conclusion - Achievements are listed and a future work is proposed.

Chapter 2

Background

2.1 Additive Manufacturing

Frazier [6] states that ASTM has defined additive manufacturing (AM) as "a process of joining materials to make objects from 3D model data, usually layer upon layer, as opposed to subtractive manufacturing methodologies. Synonyms: additive fabrication, additive processes, additive techniques, additive layer manufacturing, layer manufacturing, and freeform fabrication". Also in agreement with ISO/ASTM 52900:2015 [7] "Additive manufacturing is the general term for those technologies that based on a geometrical representation, creates physical objects by successive addition of material". Further definitions are available, but in essence is a process that involves material deposition as opposed to conventional processes that are subtractive.

AM has its advantages and limitations as any other technology and therefore is not suitable for every application. Levy et al. [8] state that Additive Manufacturing (Layer Manufacturing) is well suited to build parts that possess a medium to high geometric complexity as well as a low batch of production. In figure 2.1 is represented the aforementioned.

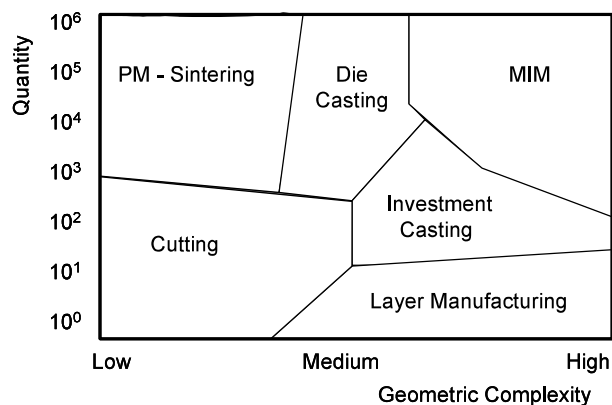


Figure 2.1: Geometric Complexity vs Quantity for metal production methods [8]

An obvious opportunity of AM is the reduction of waste material as opposed to a profound limitation of a slow manufacturing production speed. Kleer et al. [9] summarize the opportunities and limitations of

AM in a technological and economic point of view. These characteristics are represented in the following table 2.1.

Technological characteristics of AM	
Opportunities	Limitations
<ul style="list-style-type: none"> ▫ Direct digital manufacturing of 3D product designs without the need for tools or molds ▫ Change of product designs without cost penalty in manufacturing ▫ Increase of design complexity (e.g., lightweight designs or integrated cooling chambers) without cost penalty in manufacturing ▫ High manufacturing flexibility: objects can be produced in any random order without cost penalty ▫ Production of functionally integrated designs in one-step ▫ Less scrap and fewer raw materials required 	<ul style="list-style-type: none"> - Solution space limited to 'printable' materials (e.g., no combined materials) and by size of build space - Quality issues of produced parts: limited reproducibility of parts, missing resistance to environmental influences - Significant efforts are still needed for surface finishing - Lacking design tools and guidelines to fully exploit possibilities of AM - Low production throughput speed - Skilled labor and strong experience needed

Economic characteristics of AM	
Opportunities	Limitations
<ul style="list-style-type: none"> ▫ Acceleration and simplification of product innovation: iterations are not costly and end products are rapidly available ▫ Price premiums can be achieved through customization or functional improvement (e.g., lightweight) of products ▫ Customer co-design of products without incurring cost penalty in manufacturing ▫ Resolving "scale-scope dilemma": no cost penalties in manufacturing for higher product variety ▫ Inventories can become obsolete when supported by make-to-order processes ▫ Reduction of assembly work with one-step production of functional products ▫ Lowering barriers to market entry ▫ Local production enabled ▫ Cost advantages of low-wage countries might diminish in the long run 	<ul style="list-style-type: none"> - High marginal cost of production (raw material costs and energy intensity) - No economies of scale - Missing quality standards - Product offering limited to technological feasibility (solution space, reproducibility, quality, speed) - Intellectual property rights and warranty related limitations - Training efforts required - Skilled labor and strong experience needed

Table 2.1: Technological and Economic Opportunities and Limitations of AM [9]

The most usual AM processes used are divided primarily by its heat sources (beam or arc) and secondly by its type of feedstock. Martina and Williams [10] show this division schematically in the following figure 2.2.

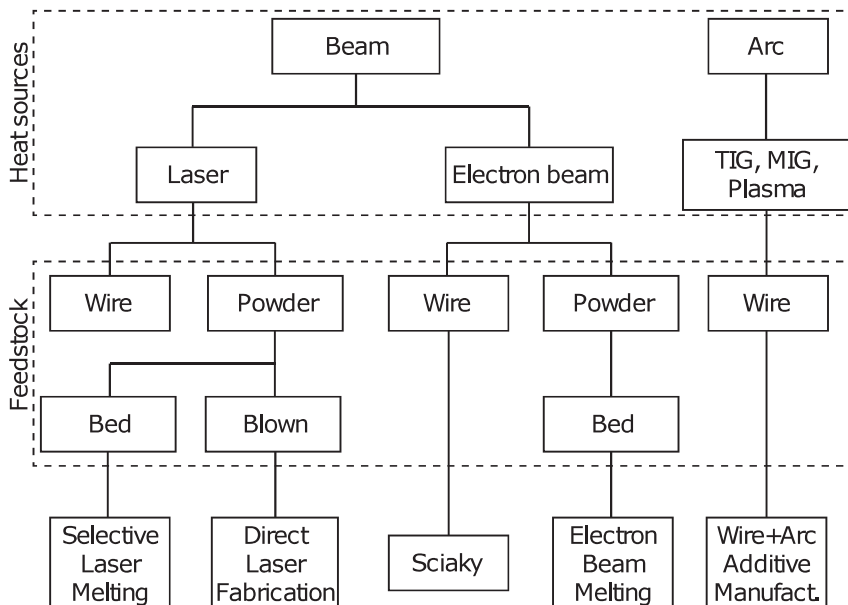


Figure 2.2: Current main AM processes [10]

As noticed in figure 2.2, the feedstock divides into wire or powder. Powder AM processes fuses metal powder material together as opposed to wire AM processes that fuses a wire spool. Ding et al. [11] perform a comparison in a form of table. The latter is shown in table 2.2.

Additive materials	Process	Layer thickness (μm)	Deposition rate (g/min)	Dimensional accuracy (mm)	Surface roughness (μm)
Powder	LC	N/A	1–30	± 0.025 – ± 0.069	1–2
	SLM	20–100	N/A	± 0.04	9–10
	SLS	75	~ 0.1	± 0.05	14–16
	DLF	200	10	± 0.13	~ 20
Wire	WAAM	~ 1500	12	± 0.2	200
	EBF ³	N/A	Up to 330	Low	High

Table 2.2: Comparison between Powder AM and Wire AM [11]

In table 2.2 a comparison between Powder and Wire AM processes is conducted. Wire AM has the advantage of possessing a greater deposition rate and a larger layer thickness when compared to Powder AM. However, the latter accomplishes better geometrical tolerances since its dimensional accuracy and surface roughness are several times lower when compared to Wire AM.

As noticed in figure 2.2, the main AM processes current in use are Selective Laser Melting (SLS), Direct Laser Fabrication (DLF), Sciaky, Electron Beam Melting (EBM) and Wire+Arc Additive Manufacturing (WAAM). In this chapter 2, arc ramification will be the one considered and therefore in the following section 2.2, wire AM processes will be addressed.

2.2 Wire and Arc Additive Manufacturing

Regarding energy sources, Ding et al. [11] classify wire-feed AM processes into three main groups: Wire and Laser Additive Manufacturing (WLAM), Electron Beam Freeform Fabrication (EBF) and Wire and Arc Additive Manufacturing (WAAM). In this section 2.2 only WAAM will be considered.

Neto [12] defined Wire Arc Additive Manufacturing (WAAM) as an Additive Manufacturing process that uses an electric arc as a heat source and wire as a feedstock. The electric arc melts the wire and deposition is performed layer by layer until a final part is achieved.

This technology was first patented in 1925 by Baker Ralph [13]. It possesses several benefits. Martina and Williams [10] and Williams et al. [14] claim the following advantages:

- Reduction of waste material
- Low initial capital cost ($\sim 90\text{k}$)
- Much lower manufacturing and production costs when compared to power-based processes
- Open architecture
- High deposition rates (1 kg/h to 4 Kg/h)
- No limitation of the part to be deposited. It only depends on the set-up used
- Possibility of integrated machining due to the increase of robotic machining as stated by Pandremenos et al. [15].

On the other hand the main issue related to WAAM is the residual stress that arises when depositing a part. It occurs due to the significant heat input that reaches high values because WAAM uses arc sources. Ding et al. [16] state that the significant heat input results in the distortion of the part when unclamped as well as in the substrate deformation. There are several ways to mitigate this main problem and are mentioned below. Williams et al. [14] present further information on these mitigation processes.

- Symmetrical building
- Back to back building
- Optimising part orientation
- High pressure interpass rolling

Regarding the materials that are able to be deposited with this technology, plenty of them are suitable. The most common are aluminium, titanium and steel alloys as stated by Castro e Silva [17].

Finally, there are three types of process that can be chosen as heat source: Gas Metal Arc Welding (GMAW), Gas Tungsten Arc Welding (GTAW) and Plasma Arc Welding (PAW). These three processes and a GMAW variant will be discussed in the following section 2.3 with a greater emphasis in the latter.

2.3 Wire and Arc Additive Manufacturing Processes

Ding et al. [11] represented the three processes aforementioned in a form of a schematic diagram represented in the following figure 2.3.

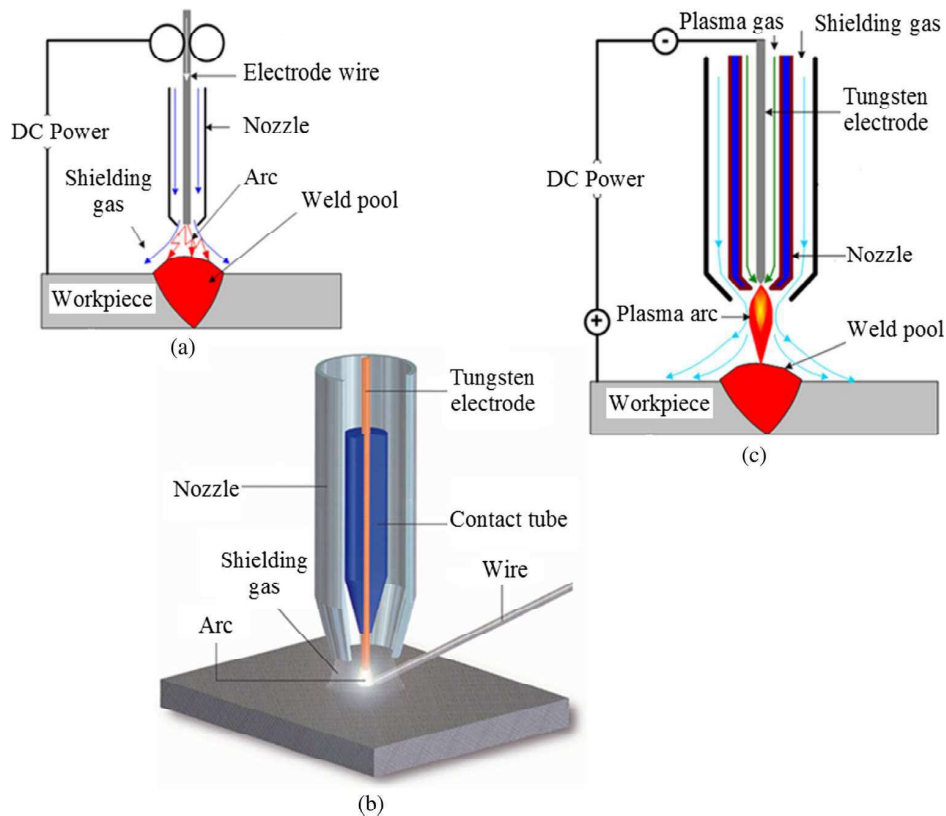


Figure 2.3: Schematic diagram of the processes - (a) GMAW, (b) GTAW and (c) PAW [11]

2.3.1 Gas Tungsten Arc Welding

According to Pires [18] and Khan [19], Gas Tungsten Arc Welding, also named as Tungsten Inert Gas (TIG), is a process where a arc is struck between a non-consumable tungsten electrode and a workpiece in order to establish a melt pool. Shielding gas is delivered through the torch, usually helium, argon or a mixture of both so that an inert atmosphere is created in order to prevent the contamination of the weld pool. Finally and because the shielding gas is conductive, the electric arc is produced by passing the current through the shielding gas, creating an arc between the tungsten electrode and the workpiece. For a better understanding observe figure 2.3 - (b).

This process is important in the deposition of titanium because the latter is affected by arc wandering. More information about the use of this process for the deposition of titanium is presented in the work performed by Wang et al. [20].

2.3.2 Plasma Arc Welding

According to Pires [21] and Khan [19], Plasma Arc Welding (PAW) has the same fundamentals of TIG. However in this case the torch possesses a water-cooled nozzle that constricts the arc, creating a concentrated ionised plasma arc. Also another difference that is evidenced in figure 2.3 - (c) is that in plasma arc welding the tungsten electrode is separated from the shielding gas chamber.

This process is also important in the deposition of titanium because of the same limitation. More information about the use of this process for the deposition of titanium is presented in work performed by Martina et al. [22].

2.3.3 Gas Metal Arc Welding

According to Pires [23] and Khan [19], Gas Metal Arc Welding (GMAW) is a fusion welding process where a consumable electrode is melted due to an arc as a heat source to form a weld pool. Usually this electrode is stored in a form of a spool.

Still according to Pires [23] and Khan [19], GMAW divides into two classes: Metal Inert Gas (MIG) and Metal Active Gas (MAG). The difference between both lies in the nature of the shielding gas. In MIG is Argon, Helium or a mixture of both, therefore there is no chemical reaction with the melt pool. In opposition to MAG, where the shielding gases are: CO₂, mixtures of Argon with CO₂ or mixtures of Argon with CO₂ and O₂. In the latter, since the gases are active, MAG promotes reactions of oxidation and reduction with the melt pool.

In the work performed by Martina and Williams [10] is stated that "MIG is the process of choice" because the welding torch is coaxial with the wire promoting an easier tool path.

In the following table 2.3 is represented the correlation between current and wire feed speed, voltage, travel speed, electrode extension, wire diameter and shielding gas with bead width, penetration, bead size and deposition rate. This correlation was performed by Duarte [24].

Parameters	Bead width		Penetration		Bead size		Deposition rate	
	<u>Increase</u>	<u>Decrease</u>	<u>Increase</u>	<u>Decrease</u>	<u>Increase</u>	<u>Decrease</u>	<u>Increase</u>	<u>Decrease</u>
Current and wire feed speed	↑	↓	↑	↓	↑	↓	↑	↓
Voltage	↑	↓	No effect	No effect	Small effect	Small effect	Small effect	Small effect
Travel speed	↓	↑	↓	↑	↓	↑	Small effect	Small effect
Electrode extension	↓	↑	↓	↑	↑	↓	↑	↓
Wire diameter	Small effect	Small effect	↓	↑	Small effect	Small effect	↓	↑
Shielding gas	↑	↓	↑	↓	Small effect	Small effect	Small effect	Small effect

Table 2.3: Effect of changes in process variables on weld attributes [24]

The preferential process to be used in WAAM is a GMAW variant process named Cold Metal Transfer (CMT) from Fronius. According to Fronius [25], this process has higher deposition rates with no increase heat input, resulting in minimal distortion and practically without any spatter. Also it produces less welding fumes improving the conditions for the welder.

Cold Metal Transfer

According to Selvi et al. [26] and Furukawa [27], Cold Metal Transfer is a modified MIG process discovered by Fronius after several years of research. The main difference of CMT is that delivers a new type of mechanical droplet cutting method. As stated by Pickin and Young [28], with this method a low thermal input and a controlled method of material deposition is achieved.

The operating principle of a CMT depends on the wire. The tip of the electrode makes contact with the workpiece and almost instantaneously the wire retracts starting the droplet transfer according to Selvi et al. [26].

In the following figure 2.4, high-speed images of a CMT droplet transfer are shown.

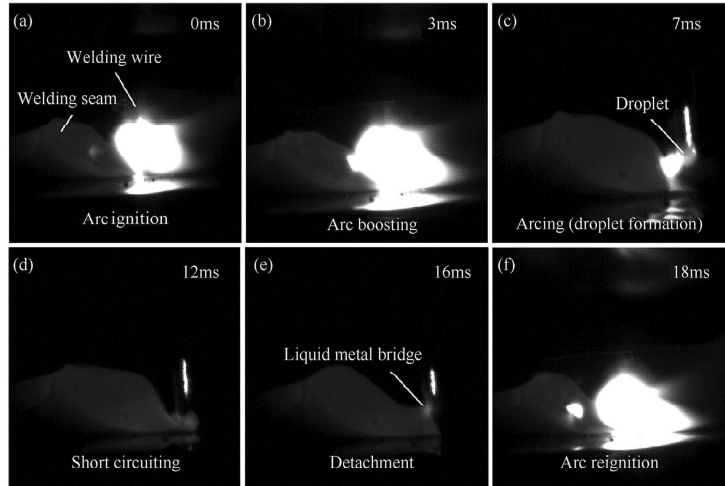


Figure 2.4: High-speed images of a CMT droplet transfer [26]

It is important to understand how the current and voltage waveform varies over time in CMT. Figure 2.5 represents the current and voltage waveforms of a CMT process.

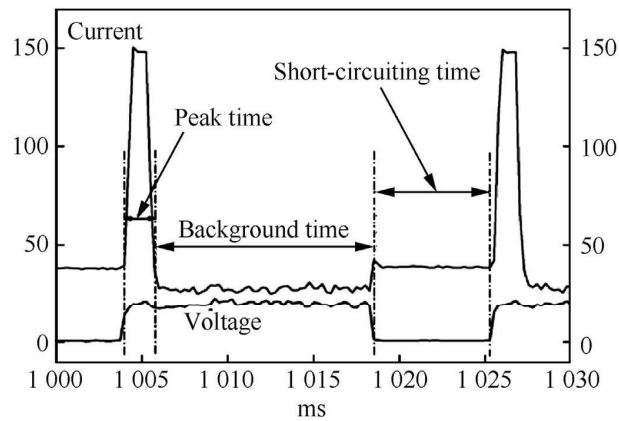


Figure 2.5: Current and Voltage waveforms of a CMT process [26]

According to Selvi et al. [26] there are three main phases:

- Peak Current Phase - in this phase the arc is ignited and the wire is heated
- Background Current Phase - this phase prevents globular droplet transfer
- Short-circuiting Phase - this phase prevents spatter and "assists in the liquid fracture and transfer of material into the welding pool"

Finally a brief comparison between MIG and CMT is carried out to perceive the advantages of such a similar process. The main advantages of CMT are:

- Low Energy
- Spatter Free - due to the decrease value of the current to near zero in the short-circuiting phase.
- High Welding Speed - due to the lower heat inputs when compared to MIG

Chapter 3

Materials and Methodology

In this chapter 3, the following aspects will be addressed:

- Materials identification and classification
- Equipments and set-ups used
- Different methodologies used throughout the work in order to acquire and analyse the data

3.1 Methodology

The methodology consists in the different systems of methods used to achieve the final part. As carried by Castro e Silva [17], the methodology of the author comprises three different blocks. The green one represents the work performed in the welding laboratory, the blue one regarding a computer and finally the orange one in the metallography laboratory. This flow-chart is represented in figure 3.1.

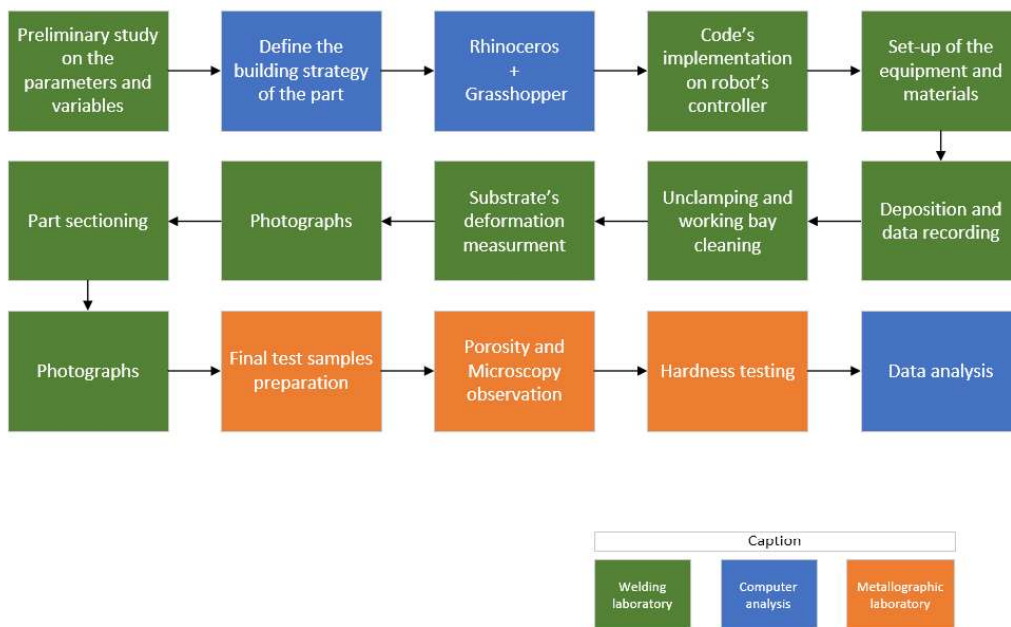


Figure 3.1: Methodology [17]

3.2 Materials

The welding consumable used was a mild steel ER70S-6 SupraMig Ultra from Lincoln Electric with a wire diameter of 1.0 mm. It was supplied in a form of a spool of 15Kg. The manufacturer data sheet of the material is presented in appendix A.

The substrate material was the 080A15 BLUE Bright Steel Flat and was provided with the following dimensions: 200mm X 12mm x 1000mm. To be used in the set-up it was cut to a new dimension of: 200mm X 250mm. The equipment operated to cut the plate was a semi-automatic horizontal bandsaw Bomar individual 610.440GH that is represented in figure 3.2.



Figure 3.2: Semi-automatic horizontal bandsaw Bomar Individual 610.440GH

Table 3.1 shows the chemical composition of the substrate and of the deposited part:

Table 3.1: Chemical composition of the substrate and of the deposited part

Material	Chemical Composition									
	C	Mn	Si	P	S	Ni	Cr	Mo	V	Cu
Wire SupraMig Ultra	0.08	1.70	0.85	0.25 máx	0.035 máx	0.015 máx	0.015 máx	0.015 máx	0.03 máx	0.50 máx
Substrate	0.13 - 0.18	0.70 - 0.90	0.10 - 0.40	0.05 máx	0.05 máx	-	-	-	-	-

According to [29], the filler material "Type ER70S-6 is a wire with higher levels of Deoxidizers (Mn and Si) compared to other carbon steel wires. This wire is suitable for welding of steels with moderate amounts of scale or rust."

In the same document is mentioned that: "For Mig welding use Carbon Dioxide or Argon + CO₂ or Argon + 2% Oxygen as shielding gases.". In fact the shielding gas used through experiments was a SPECSHIELD 20% CO₂ in ARGON - ISO 14175-M21-ArC-20 with a constant pressure of 5 bar.

3.3 Equipment Set-up

Two set-ups were assembled in order to achieve the objective of this work. The first one was used to obtain the data for the largest and smallest dimension of the final part. As opposed to the second which was used to fine tune the parameters acquired and to build the final part.

The first set-up is shown in figure 3.3.

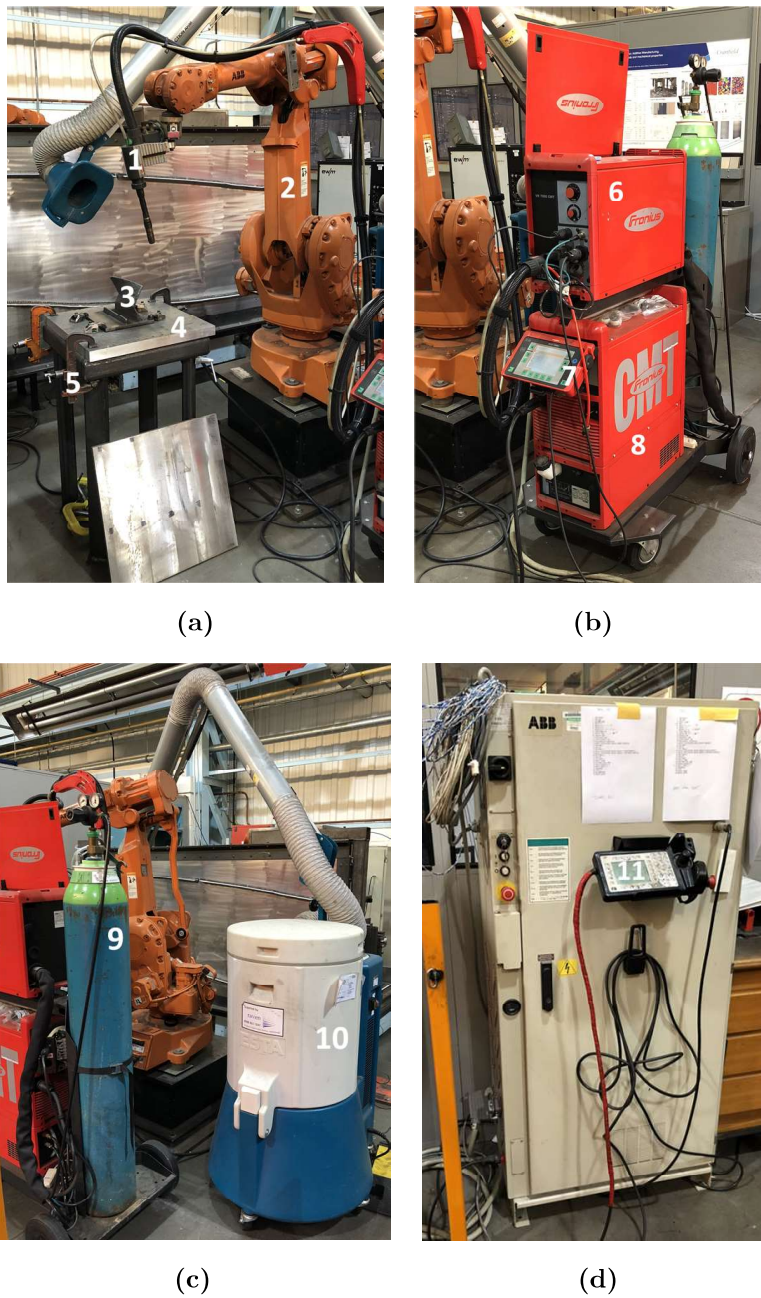


Figure 3.3: First Set-Up

The label of figure 3.3 is:

1. Torch
2. 6-axis Robot - ABB IRB 2400 M96
3. Part
4. Substrate
5. Clamps

6. Arc Wire Feeder - Fronius VR 7000 - CMT 4R/G/W/F++
7. CMT Power Source Controller - Fronius Fernbedienung RCU 5000i Univ.SD
8. Cold Metal Transfer Power Source - Fronius CMT Advanced 4000 R)
9. Compressed Shielding Gas Bottle - BOC Gases Specshield 20% CO₂, Ar
10. Local Exhaust Ventilation - ESTA SRF - K 10 FM 55 203
11. Robot Controller

The second set-up is represented in the following figure 3.4.



(a)



(b)



(c)



(d)

Figure 3.4: Second Set-Up

The label of figure 3.4 is:

1. 6-axis Robot - KUKA KR 150 L110-2 F 2000
2. Arc Wire Feeder - Fronius VR 7000 - CMT 4R/G/W/F++
3. CMT Power Source Controller - Fronius Fernbedienung RCU 5000i Univ.SD
4. Cold Metal Transfer Power Source - Fronius CMT Advanced 4000 R
5. Torch
6. Substrate
7. Clamps
8. Robot Controller
9. Compressed Air Bottle - BOC
10. Compressed Shielding Gas Bottle - BOC Gases Specshield 20% CO₂, Ar
11. Local Exhaust Ventilation - ESTA SRF - K 10 FM 55 203

Both set-ups differ with respect to the employed robot and displacement of the equipment. However both are assembled with the same principles.

3.4 Deposition Parameters

Several experiments were performed in order to acquire the final parameters.

The first data of parameters was obtained using the first set-up (figure 3.3). The experiment was performed to test the feasibility of the parameters in order to deposit the largest and the smallest sections of the part to be delivered.

The following figure 3.5 exhibit the experiments performed for the largest section existent in the final part.



Figure 3.5: Experiment performed for the largest section

The following figure 3.6 presents the final experiment for the smallest section:



(a)

(b)



(c)

Figure 3.6: Experiment performed for the smallest section

On the other hand the second data of parameters was obtained using the second set-up (figure 3.4). In this case the main fine tuning was employed in order to obtain an acceptable and constant deposition in the intersection areas. The following figure 3.7 shows a few experiments performed:



(a)



(b)



(c)



(d)

Figure 3.7: Experiments performed to obtain the intersections

The results and the data of such experiments to obtain the final set of parameters will be discussed further more in chapter 4.

3.5 Deposition of the Part

Layers were produced by depositing oscillated passes and alternating the direction of deposition between each layer.

As aforementioned, various experiments were performed. For each layer deposited, a common procedure and data collection was applied:

- The part was let to cool down between each layer. The set interlayer temperature was around 70°C in order to start depositing again. The temperature was measured with a RS Pro Digital Thermometer 206 - 3722 (figure 3.8 - (a)).



(a)



(b)

Figure 3.8: (a) RS Pro Digital Thermometer 206 - 3722, (b) Digital Calliper SPI 12-527-8

- Between each layer, measurements of the layer height were undertaken in order to keep track of the height of the building part to guarantee that the final part would have the exact same height that the required one. In the beginning the measurement equipment was a Digital Calliper SPI 12-527-8 (figure 3.8 - (b)). However the maximum measurement capability of this equipment is $150mm$. With the objective to continue to register the height, a more archaic method was used. The second equipment used was a common ruler.

3.6 Path Generator

Every deposition was planned using WAAM software from Cranfield University. Notice that this was a Beta version and one objective of this work was to contribute to the software development.

The software uses two other programs - Rhinoceros and Grasshopper. According to [30], Grasshopper is "a graphical algorithm editor tightly integrated with Rhino's 3-D modeling tools". On the other hand, stated by [31], Rhinoceros can "create, edit, analyze, document, render, animate, and translate NURBS* curves, surfaces, and solids, point clouds, and polygon meshes. There are no limits on complexity, degree, or size beyond those of your hardware". In this work Rhinoceros presents the CAD model, the layers and the deposition paths. On the other hand, in the Grasshopper the user is able to define the parameters of the path.

The post-processor defined in the Grasshopper, in this case for KUKA, will generate code files for each layer. These files will have to be input into the operating system in order to deposit the part.

In the following figure 3.9 is represented the interface of Rhinoceros.

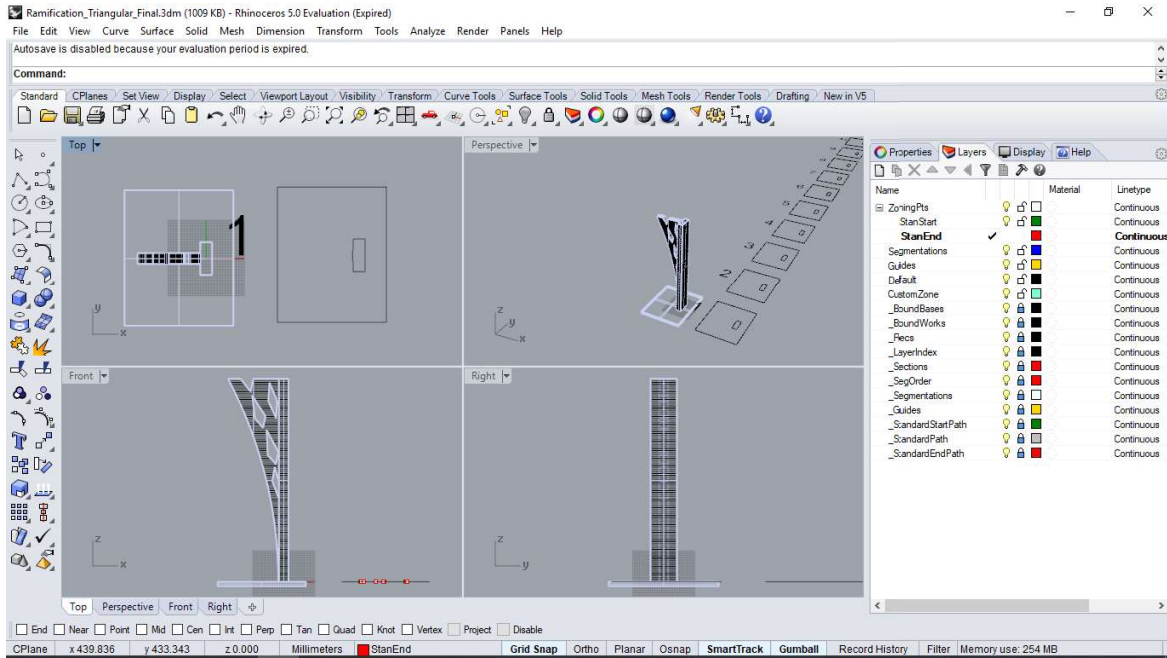


Figure 3.9: Rhinoceros software interface

As it can be observed in figure 3.9, in this interface there are four types of views (top, perspective, front and right). It can be chosen the one that is more convenient for the user. On the right side of the figure 3.10 there are five layers designations that are important.

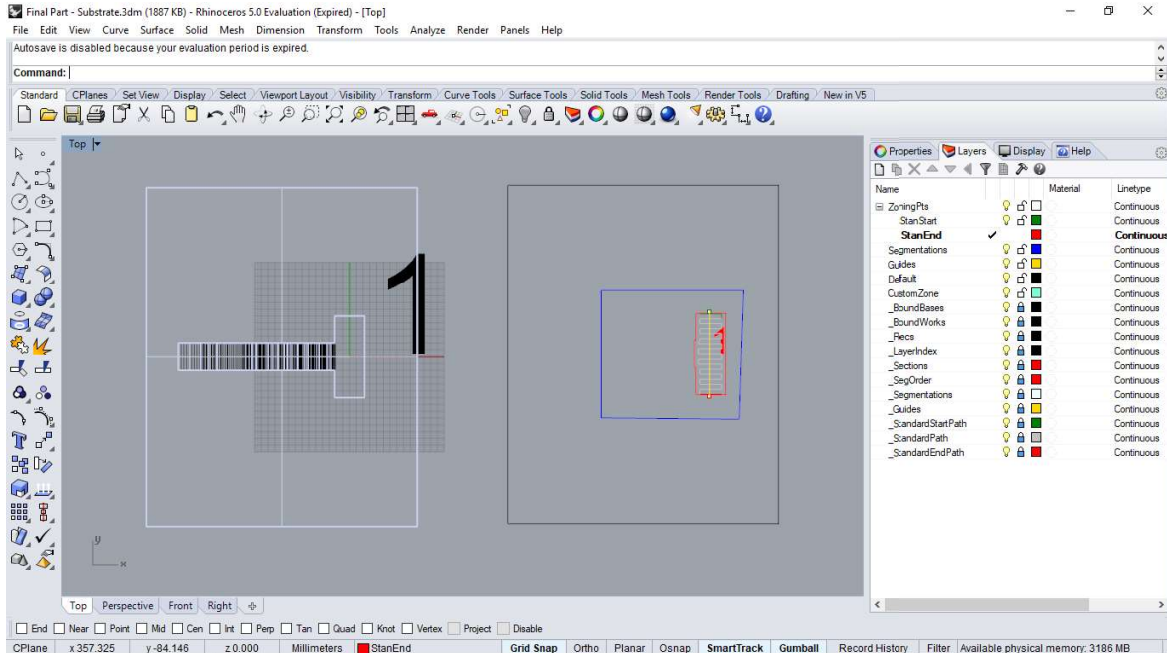


Figure 3.10: Representation of the layers in Rhinoceros

The user uses them in the following order:

- "Segmentations" - The user draws a dark blue box to define the region of the CAD model where the path will be defined. Once it is drawn the number of the section appears in red (in this case is

the number 1).

- "Guides" - It is represented by the yellow line. This line sets up the direction of the oscillated path. The latter is perpendicular to the line drawn so the user must be aware of such information.
- "ZoiningPts" - There are two points in the figure. A starting one that is characterized by the green colour and a stopping one characterized by the red colour. Once both of these points are defined, the oscillated path appears in the interface.
 - StanStart - As the designation states is a starting position point, therefore when depositing the torch will start welding in that position.
 - StanEnd - On the other hand will stop at this position.
- "CustomZone" - This last one is characterized by a bright blue box and is only used when a particular part of the path needs different parameters of deposition. This feature was not used in the experiments as well as in the building of the final part.

In the following figure 3.11 is represented the interface of Grasshopper.

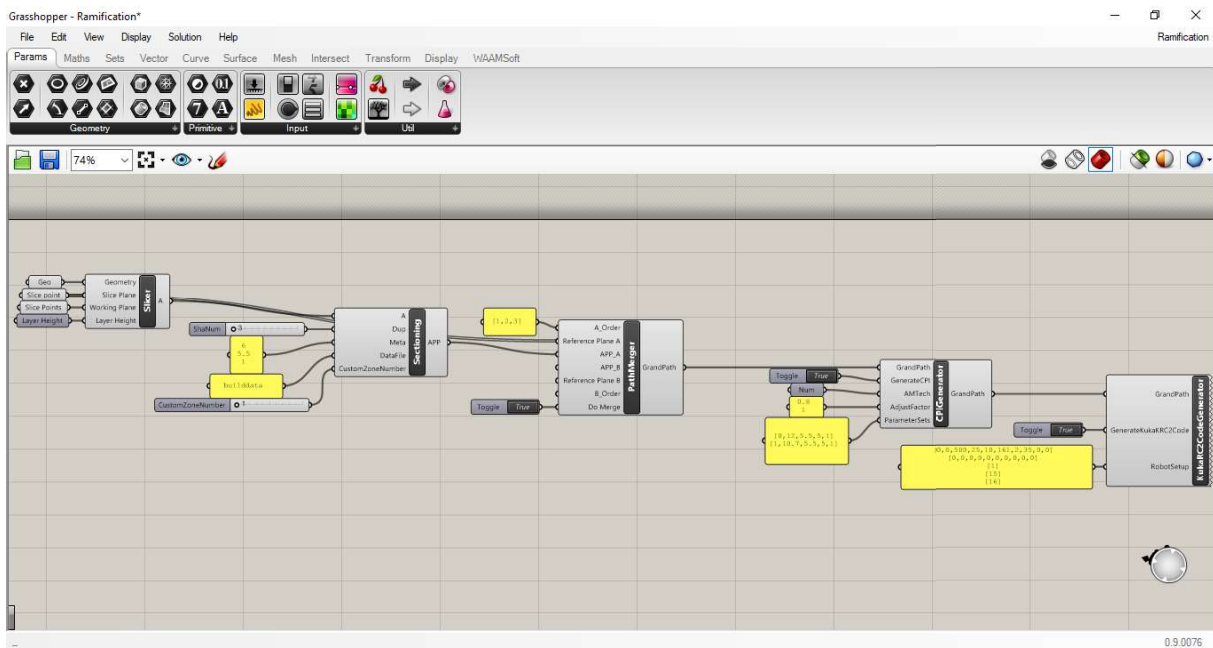


Figure 3.11: Grasshopper software interface

In this interface there are five main blocks:

- "Slicer" - As can be observed, entries in this main block define the: "Geometry", "Slice Plane", "Working Plane" and "Layer Height". These are defined with the following four commands:
 - "Geo" - Once the user uses this block, it needs to choose the CAD model displayed in Rhinoceros interface.

- "Slice point" - The user selects the position of the slicing of the layer in one of the views of Rhinoceros. In figure 3.10, in the "Perspective" view, the slicing can be observed.
 - "Slice Points" - In this command the user defines three points in order to define the plane from which the upwards slicing begins.
 - "Layer Height" - The user sets a value for the layer height. That will be the spacing between each layer.
- "Sectioning" - This main block has five input variables:
 - "A" - The user connects this point to the output variable of the "Slicer" main block. It is just a connection variable.
 - "Dup" - This variable stands for duplication. It is connected to a block "ShaNum". The user is able to change the input number so that the software is capable to apply that amount of duplications. This tool is very helpful because several consecutive slicing layers have the same deposition parameters and shape.
 - "Meta" - There are three basic parameter values in this box. The first one is the bead width of the oscillated path. The second one is the wire feed speed (m/min). The last and third one is the wire diameter (mm).
 - "DataFile" - The data file is the place where the software saves all the build data. There will be a file with the designation written in this box. In this case - "bulddata".
 - "CustomZoneNumber" - This variable is connected to a box with the exact same name. However in the latter the user inputs a number of how many "CustomZone" will be used in Rhinoceros interface.
 - "PathMerger" - This main box is used to define the deposition order of the segmentations as well as to merge the information when a symmetrical building occurs. In the case of these experiments, only one side was used. Therefore the variables "APP_B", "Reference Plane B" and "B_Order" were not used.
 - "A_Order" - In this box is introduced the order of the segmentations created in the Rhinoceros interface. This information will allow the software to know, in every slicing, where to begin.
 - "Reference Plane A" - This variable is the same as set-up in the "Slice Plane" in the "Slicer" box.
 - "APP_A" - This is the output variable from the "Sectioning" box.
 - "Do Merge" - It is connected to a toggle that allows the information of the previous boxes to pass to the following one when is true. On the other hand when is false does not allow.
 - "CPIGenerator" - This main block has five input variables:
 - "GrandPath" - This is the output variable of the "PathMerger" box.
 - "GenerateCPI" - This toggle has the same function of the "Do Merge" one.

- "AMTech" - In this box a value is defined. If the user employs a plasma source the input number must be the value 1, if uses CMT the value is 2.
- "AdjustFactor" - It is the ratio between the velocity required and the nominal velocity for the first layers. This is an important value because the substrate is cold than it should be, so the user needs to slow down the travel speed in order to accommodate more heat so that the layer stays flat and bonds well with the substrate.
- "ParameterSets" - The box connected to this variable has five more input values. It can be input as many sets of values as requested. By order the variables are:
 - * Index Number - By default the parameters of the path are the ones that correspond to the index number zero. The following index numbers created are used to define the parameters of the corresponding custom zones;
 - * Current - Since it was used CMT, the current was specified in the CMT power source controller. If Plasma was employed, then it should be defined in this variable;
 - * Wire Feed Speed;
 - * Travel Speed;
 - * Job Number - This value must match the number that appears in CMT power source controller.
- "KukaRC2CodeGenerator" - It is the last main block and generates the code to be read by the Kuka robot. It generates a .txt file for each layer. In appendix B.1 an example of a builddata file can be observed.
 - "GrandPath" - This is the output variable of the "CPIGenerator".
 - "GenerateKukaRC2Code" - This variable is connected to a toggle. Its function was already explained.
 - "RobotSetup" - In this box the home position of the robot is defined.

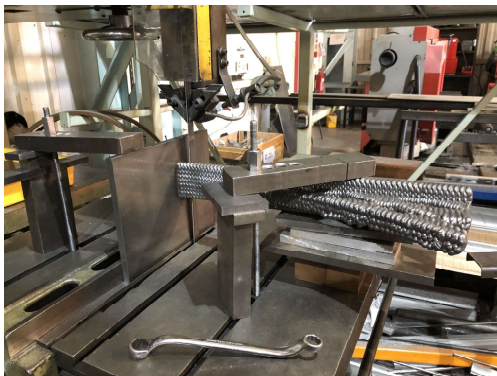
3.7 Samples Preparation

3.7.1 Sample Study Region

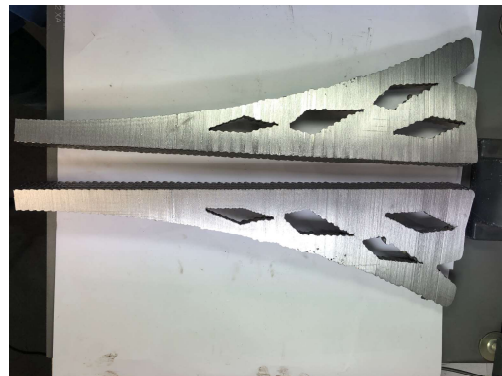
The final part was cut into half along its symmetrical axis in order to use a side for display purposes and the other for further testing. The equipment used for the main cut was a Startrite 316 represented in figure 3.12. In figure 3.13 is represented the final cutting process.



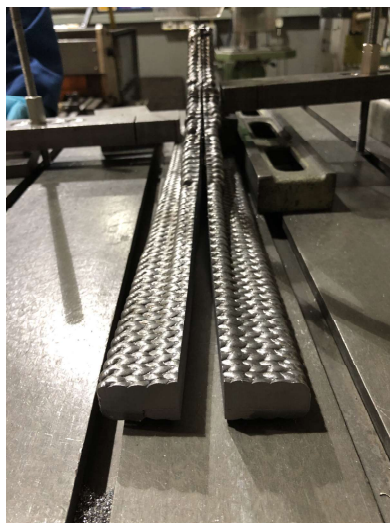
Figure 3.12: Startrite 316



(a)



(b)



(c)

Figure 3.13: Final part cutting process

After the main cut, smaller sections were cut with the help of a Struers Discotom - 60 (figure 3.14) in order to obtain a cleaner sectioned part.



Figure 3.14: Struers Discotom - 60

The critical zones were chosen to be studied such as the joining regions as well as other important sections. The following figure 3.15 represents the studied areas of the final part:

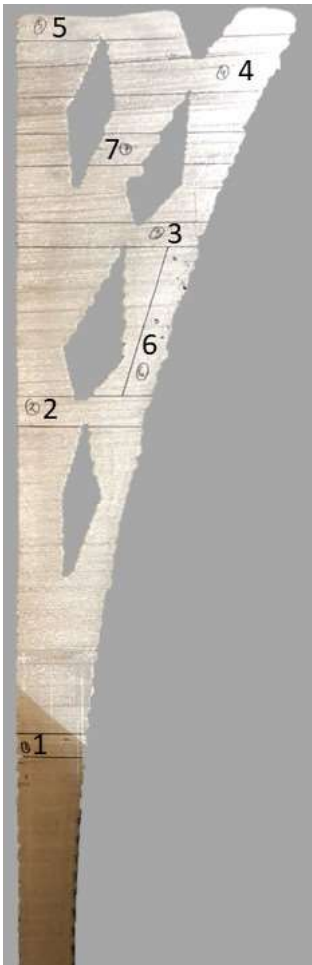


Figure 3.15: Regions of interest of the final part

Regions of interest:

- Base - 1
- Mid-intersection sections - 2, 3, 4 and 5
- Visible porosity defects - 6
- Smallest thickness wall region - 7

3.7.2 Samples Preparation Methodology

After choosing the regions of interest, the next step was the preparation of the samples for the next stage. This step was performed in the metallography laboratory.

The procedure is:

1. Cold-mounting the 40mm and 30mm cylinder moulds.
2. Grinding the moulds with different grit sandpaper values using an ATA Saphir 520 (figure 3.16).
Each grinding stage has a duration of 2:30 minutes. In total there are four grinding stages:
 - 120 grit stage
 - 240 grit stage
 - 1200 grit stage
 - 2400 grit stage



Figure 3.16: ATA Saphir 520

3. Polishing the moulds with a proper polish magnetic plate using the same equipment and using a polishing agent. Once again this stage has a duration of 2:30 minutes.
4. After the polish, the samples are washed with a soap agent and afterwards with alcohol in the following workstation (figure 3.17).



(a)



(b)

Figure 3.17: Washing workstation (a) Water washing workstation (b) Alcohol washing workstation

5. After the cleaning process the samples are dried with the help of a MetPrep sample drying station (figure 3.18)



Figure 3.18: MetPrep sample drying station

6. The final stage is the etching that was performed by an authorized staff member.

3.8 Macro and Microscopy Observation

Once the procedure was finalized for all the samples, the next step was to search for defects, such as porosities, cracks or lack of fusion. This troubleshooting was performed using two types of observation. Both macro and microscopic observation were performed using a Nikon Optishot microscope (figure 3.19).



Figure 3.19: Nikon Optishot microscope [32]

In the macroscopic observation a Schott KL 1500 electronic was used to aid in the lightening of the samples for further image acquisition (figure 3.20).



Figure 3.20: Schott KL 1500 electronic [33]

In the microscopic observation various magnificent lenses were applied in order to attempt to find any defects.

3.9 Hardness Test

A hardness test was conducted in order to obtain an estimation of the Ultimate Tensile Strength (UTS) and Yield Strength (YS) of the final part to verify if complies with the traditional methods. Vickers micro hardness has a straight correlation with the UTS and YS. This correlation is further explained in chapter 4.

The equipment used was a Zwick Roell ZHV represented in figure 3.21.

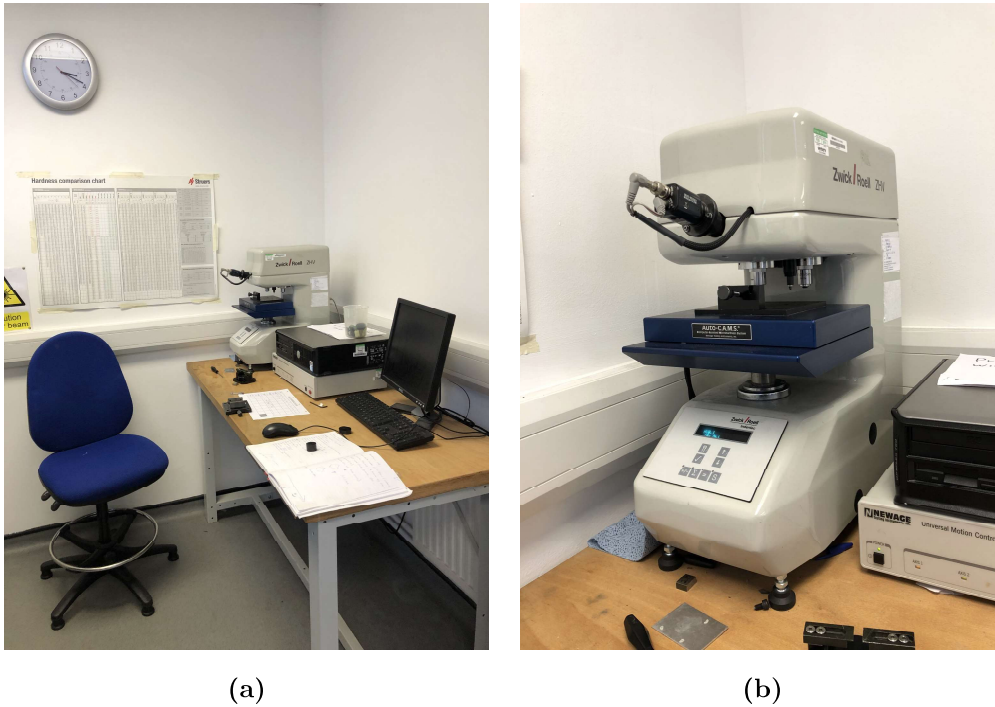


Figure 3.21: Hardness test set-up and equipment (a) Hardness test set-up (b) Zwick Roell ZHV

Per sample, 10 points were obtained with a 1mm spacing between each one. The load of the diamond indenter was 100g and the duration of the dwell time was 15 seconds per point. In figure 3.22 is possible to observe the diamond indentation at a microscopy level as well as the lines that the software uses in order to calculate the micro hardness.

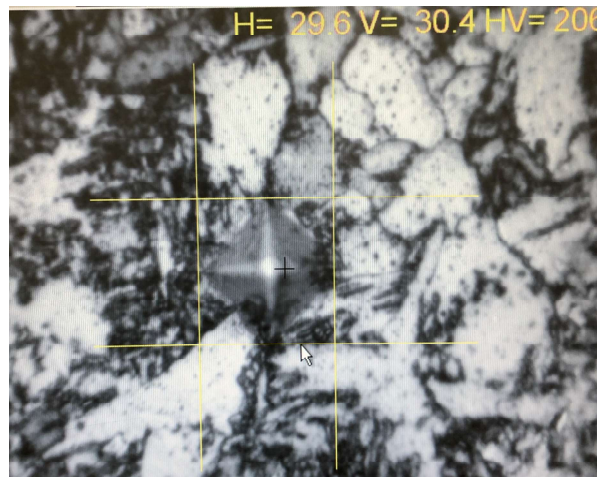


Figure 3.22: Software for the calculation of micro hardness

3.10 Path Efficiency and Substrate Deformation

Path efficiency relates to the Arc-On and Arc-Off times. Arc-On is when the deposition is actively occurring. It is the time-frame where the productive part is being carried. The Arc-Off is when the dead times occur, such as the cool-down of the part or the movement of the robotic arm to a new deposition

position. The sum of these two times result in the total time of a layer's deposition.

The time measurements were performed using a stopwatch and for every ten layers.

The substrate deformation is the amount of deformation that the substrate suffers. The deformation was measured with the help of a Digital Calliper SPI 12-527-8 (figure 3.8 - (b)).

In chapter 4 a more in depth analysis will be performed regarding path efficiency and substrate deformation.

Chapter 4

Results and Analysis

In this chapter 4, results acquired will be analysed and further discussed. A deposition parameters study will be performed for the experiments carried as well as for the final part. A macro and microscopic analysis will be undertaken. Finally a micro hardness, a path efficiency and a substrate deformation analysis will be carried out.

4.1 Deposition Parameters

In this section 4.1, results and knowledge were acquired primarily based on four stages as aforementioned.

Since CMT, variables (current, voltage and wire feed speed) and WAAM software controls the movement and other variables of the robot, the main focus was on studying and achieve the best parametrization possible.

4.1.1 First Stage

The base of the part to be deposited had the largest dimensions regarding length and width. Therefore was an important part of the structure to be studied. It was the first stage of the experiments.

The first stage was performed using the first set-up (figure 3.3). The dimensions of the base of the part were taken into consideration in order to choose the best parameters since usually the base of a WAAM part is larger when compared to the top. In this case it occurs the opposite. The deposited part is thinner in the base and increases its dimensions as the height increases. To increase the complexity of the part, the latter possess various intersections and elements that require a free form type of deposition. In the following figure 4.1 are presented the dimensions of the base of the final part ($60mm \times 20mm$).

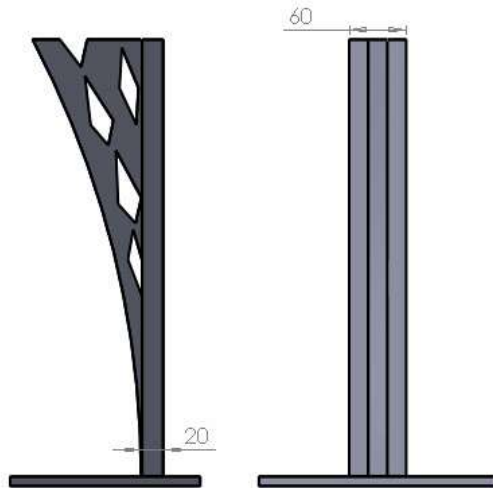


Figure 4.1: Dimensions of the base of the final part

Figure 4.2 displays the experiments performed in order to achieve the best parameters for the base of the final part.



Figure 4.2: Experiments performed for the parametrization of the base of the final part

Parameters employed in each experiment as well as the dimensions are shown in the following tables 4.1 and 4.2.

Table 4.1: Parameters used in the first stage of the experiments

Experiments	Variables					
	CTWD [mm]	Shielding Gas Flow Rate [L/min]	WFS [m/min]	TS [mm/s]	IC [A]	IV [V]
1	13	15	2.5	0.4	75	8.6
2			5.0	7.0	120	11.5
3			5.0	7.0	120	11.5
4			5.5	7.0	111	12.0
5			5.5	4.0	111	12.0
6			5.5	3.0	111	12.0
7			4.5	3.0	95	11.0
8			5.5	2.5	111	12.0
9			4.5	1.0	95	11.0
10			4.0	2	146	22.5

Table 4.2: Dimensions of the experiments of the first stage

Variables	Experiments									
	1	2	3	4	5	6	7	8	9	10
Length [mm]	-	72.11	66.77	64.93	65.25	66.00	64.66	67.23	76.49	66.30
	-	72.63	66.97	65.11	65.37	66.31	64.72	67.44	77.80	66.34
	-	72.66	67.07	65.45	65.88	66.59	65.28	67.47	78.55	67.29
Average Length [mm]	-	72.47	66.94	65.16	65.50	66.30	64.89	67.38	77.61	66.64
% of Deviation	-	20.78%	11.56%	8.61%	9.17%	10.50%	8.14%	12.30%	29.36%	11.07%
Width [mm]	-	31.05	25.43	23.59	24.61	24.47	23.71	25.65	30.24	23.93
	-	31.69	25.47	24.53	24.73	25.24	24.02	26.62	30.29	24.02
	-	33.44	26.14	24.85	24.75	25.48	24.03	27.13	30.57	24.35
Average Width [mm]	-	32.06	25.68	24.32	24.70	25.06	23.92	26.47	30.37	24.10
% of Deviation	-	60.30%	28.40%	21.62%	23.48%	25.32%	19.60%	32.33%	51.83%	20.50%
Thickness [mm]	-	4.33	4.54	3.48	4.19	5.41	4.65	5.78	7.84	5.75
	-	4.51	4.63	3.68	4.36	5.48	4.68	5.85	8.71	5.77
	-	4.71	4.66	3.82	4.41	5.49	4.92	6.31	8.85	6.58
Average Thickness [mm]	-	4.52	4.61	3.66	4.32	5.46	4.75	5.98	8.47	6.03
% of Deviation	-	29.05%	31.71%	4.57%	23.43%	56.00%	35.71%	70.86%	141.90%	72.38%

As can be observed in table 4.2, the smallest deviation percentages of the main variables are highlighted at green for a better understanding. On the other hand the largest are highlighted at red. The experiment number 7 has the smallest deviation regarding length and width, however has the fifth largest with respect to the layer height. The experiment number 9 has the largest deviation in respect to the deviation of

length and width. Finally, the largest deviation regarding width can be observed in experiment number 2. The experiments number 4 and 5 are the ones with the best compromise regarding all the main variables, however the experiment number 4 has a smaller deviation in respect to the layer height. The experiments represent a first layer, therefore a high thermal gradient is implied from the part to the substrate because the latter is still cold. A lower layer height in the following layers will arise as the thermal gradient decreases, meaning that the layer height of the experiment number 4 in the end could be lower than the layer height required. Thus, the variables chosen at this stage were the ones from experiment number 5.

4.1.2 Second Stage

The second stage was performed in order to study the smallest dimension of the final part located in the intersections. Figure 3.6 pictures some experiments performed at this stage.

In the table 4.3 are presented the parameters applied in the second stage of the experiments. This stage was performed to achieve the main parametrization for the smallest dimension of the final part as already highlighted in previous chapters.

Table 4.3: Parameters applied in the second stage of the experiments

Experiments	Variables							
	CTWD [mm]	Shielding Gas Flow Rate [L/min]	WFS [m/min]	TS [mm/s]	Cool Time [s]	IC [A]	IV [V]	Defective Layer
1	13	15	4	5	30	91	10.7	14
2					30			14
3					60			14
4					120			18
5					120			21
6					240			21
7					240			-

As observed in table 4.3, defects arose in the beginning layers of the first six experiments of the second stage. The first explanation encountered was that this defects were due to the decreasing of the thermal gradient, resulting in a higher heat accumulation in the deposited layer. This increase would lead to the defect. However upon further investigation, it was found that this defect was due to lack of fusion. These happened because the layer height that was set in the programme was higher than the actual layer height of the deposited part. Once the layer height set in the programme was reduced, the problem was solved and the experiment number seven did not possess any defects. An example of an ABB programme is presented in appendix B.2.

4.1.3 Third Stage

Third stage was the final verification and fine tune of the parameters of the previous stages. This stage was only performed to achieve the best parametrization for the first layers of the final part. In this stage four experiments were performed with a deposition of 10 layers per experiment. After this stage

the parameters for building the final part were chosen.

First Experiment

Figure 4.3 shows the first experiment.



Figure 4.3: Third stage - First experiment

In the following table 4.4 are presented the parameters of the first experiment and its values.

Table 4.4: First experiment parameters of third stage

Parameters	Values
Contact Tip to Work Distance [mm]	14
Shielding Gas Flow Rate [L/min]	20
Interlayer Temperature [°C]	80
Wire Feed Speed [m/min]	5.5
Travel Speed [mm/s]	4
Initial Current [A]	168
Initial Voltage [V]	11.6
Layer Height [mm]	4.5

Second Experiment

Figure 4.4 shows the second experiment.

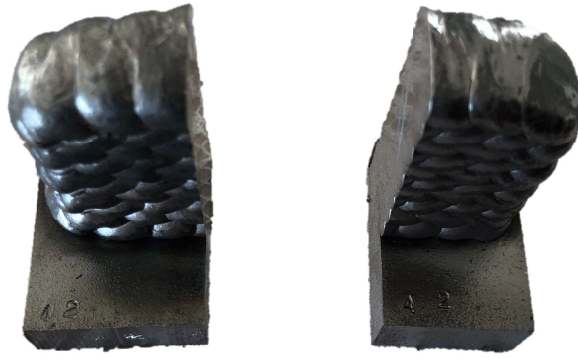


Figure 4.4: Third stage - Second experiment

In the following table 4.5 are presented the parameters of the second experiment and its values.

Table 4.5: Second experiment parameters of third stage

Parameters	Values
Contact Tip to Work Distance [mm]	14
Shielding Gas Flow Rate [L/min]]	20
Interlayer Temperature [°C]	80
Wire Feed Speed [m/min]	5.5
Travel Speed [mm/s]	5
Initial Current [A]	168
Initial Voltage [V]	11.6
Layer Height [mm]	3.5

Third Experiment

Figure 4.5 shows the third experiment.



Figure 4.5: Third stage - Third experiment

In the following table 4.6 are presented the parameters of the third experiment and its values.

Table 4.6: Third experiment parameters of third stage

Parameters	Values
Contact Tip to Work Distance [mm]	14
Shielding Gas Flow Rate [L/min]]	20
Interlayer Temperature [°C]	80
Wire Feed Speed [m/min]	6
Travel Speed [mm/s]	4
Initial Current [A]	179
Initial Voltage [V]	12.2
Layer Height [mm]	4

Fourth Experiment

Figure 4.6 shows the fourth experiment.



Figure 4.6: Third stage - Fourth experiment

In the following table 4.7 are presented the parameters of the fourth experiment and its values.

Table 4.7: Fourth experiment parameters of third stage

Parameters	Values
Contact Tip to Work Distance [mm]	14
Shielding Gas Flow Rate [L/min]]	20
Interlayer Temperature [°C]	80
Wire Feed Speed [m/min]	5.5
Travel Speed [mm/s]	4
Initial Current [A]	168
Initial Voltage [V]	11.6
Layer Height [mm]	3.8

Experiments Comparison

Table 4.8: Experiments comparison

Variables	Experiments			
	I	II	III	IV
Length [mm]	70.67	66.42	68.58	67.22
	70.81	65.88	68.72	67.35
	71.00	65.57	68.86	67.67
Average Length [mm]	70.83	65.96	68.72	67.41
% of Deviation	18.04%	9.93%	14.53%	12.36%
Width [mm]	19.51	19.97	21.43	21.95
	19.72	20.01	21.51	22.04
	19.93	20.05	21.63	22.08
Average Width [mm]	19.72	20.01	21.52	22.02
% of Deviation	1.40%	0.05%	7.62%	10.12%
Height [mm]	36.08	37.98	41.75	39.89
	36.24	38.03	42.03	40.25
	36.39	38.18	42.12	40.85
Average Height [mm]	36.24	38.06	41.97	40.33
% of Deviation	9.47%	8.75%	4.92%	6.13%

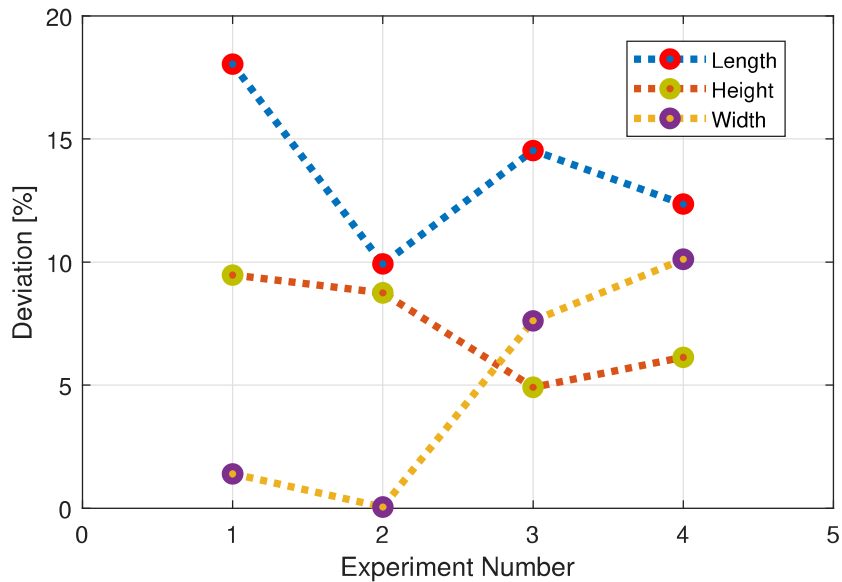


Figure 4.7: Experiments comparison graph

As observed in table 4.8 and in graph 4.7, the second experiment is the one that exhibits the lowest percentage of deviations with respect to the length (9.93%) and the width (0.05%). On the other hand, the percentage of deviation of the height is not the lowest (8.75%) but is a normal deviation that can be further mitigate once the deposition becomes stationary. Therefore it was the experiment chosen to be analysed. It is also why the experiment is cut in half in figure 4.4. The results of the macro and microscopic analysis will be discussed in section 4.3.

4.1.4 Fourth Stage

The final and fourth stage was the most challenging in order to achieve the final intersections.

In the following figure 4.8 are shown the CAD models for part to be achieved and for the part actually deposited.

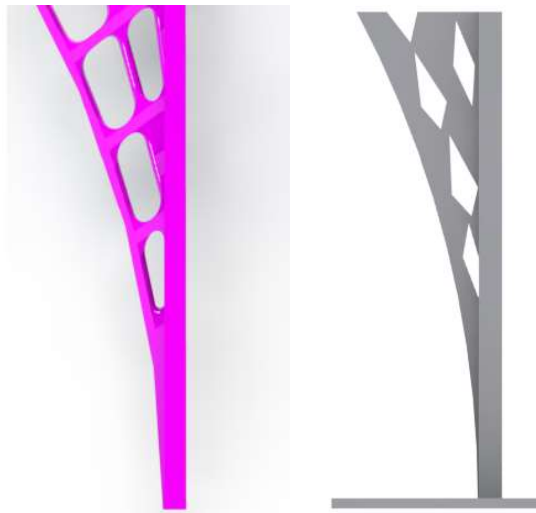


Figure 4.8: CAD comparison between the part to be achieved and the part actually deposited (a) Part to be achieved (b) Final part

Along this section 4.1.4 it will be explained the reason behind the difference between the part to be achieved and the actually deposited one.

In this stage, various experiments were performed in the interest of achieving a good joining in the closure sections. However only five will be discussed. Deposition parameters remained the same in all five experiments and are the same as the ones chosen for the second experiment of the third stage (table 4.5).

First Experiment

In the first experiment the part to be achieved was the one represented in figure 4.8 - (a). The outcome of the first experiment is shown in figure 4.9.

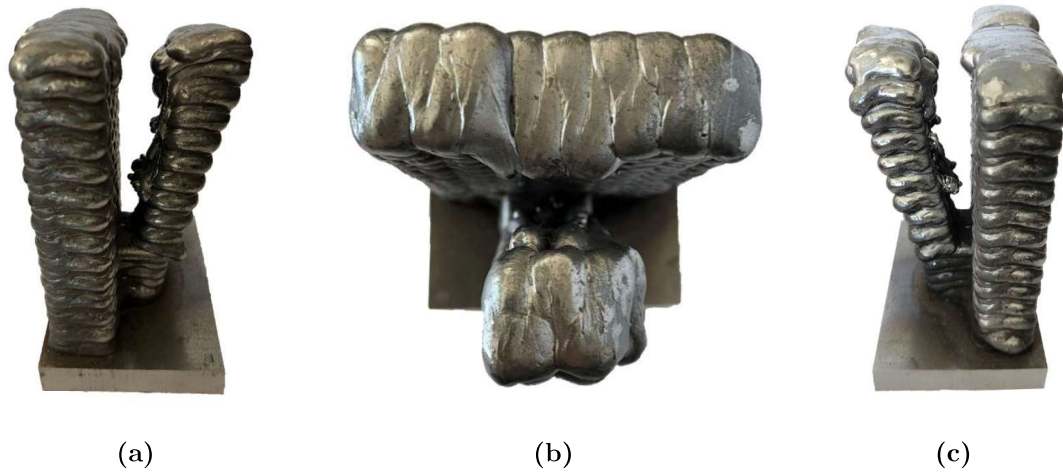


Figure 4.9: Fourth stage - First experiment

The second degree curve was too extreme to be achievable. This led to the part not closing. In figure 4.9 - (a) and (c) some small protrusions are noticeable. These occur because the overhanging was too high, therefore the wire kept feeding and created these protrusions instead of carrying on with the deposition in order to achieve a final closure.

Some similar experiments were performed, however the outcome was always identical. Thus, it was concluded that this type of deposition was not feasible. That is why the final part is different from the part to be achieved (figure 4.8).

As can be observed in figure 4.8 - (b), the opening areas of the part are lozenged. Therefore, the solution was to build the part this way with incremental layer lengths. However more experiments were performed since the closing angle of each lozenged region is a variable very important for the desired outcome.

Second Experiment

Second experiment is represented in figure 4.10.

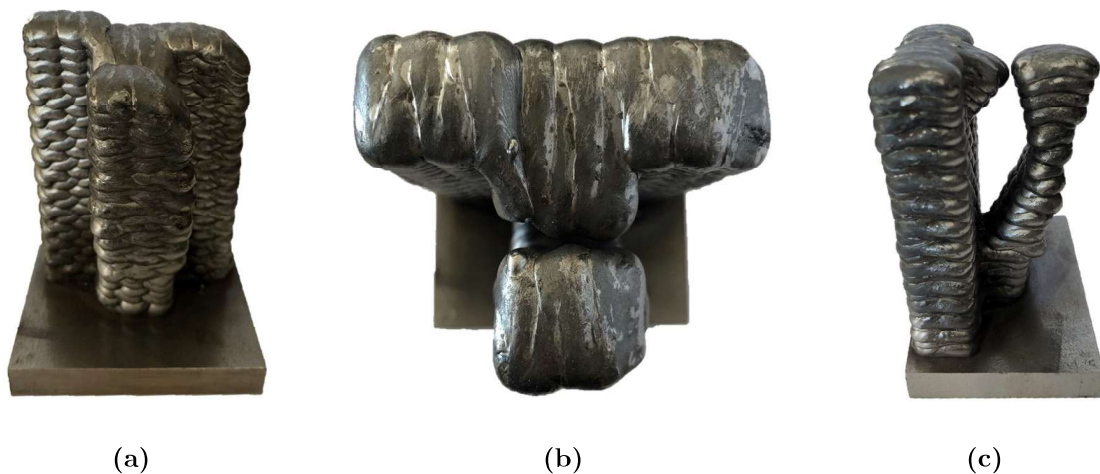


Figure 4.10: Fourth stage - Second experiment

This was the first experiment where the angle of closure was a studied variable. CAD model of this experiment is represented in figure 4.11.

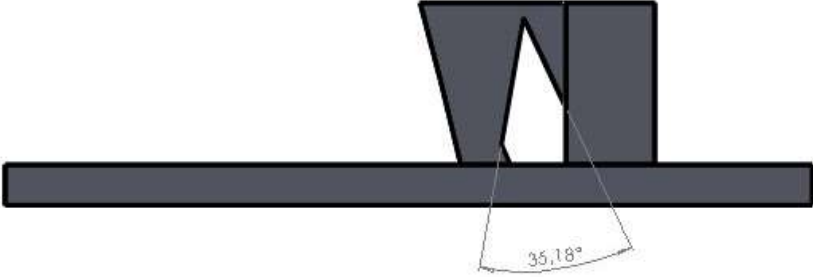


Figure 4.11: Angle of closure of second experiment

In this experiment the lozenge did not close.

Third Experiment

Third experiment is represented in figure 4.12.

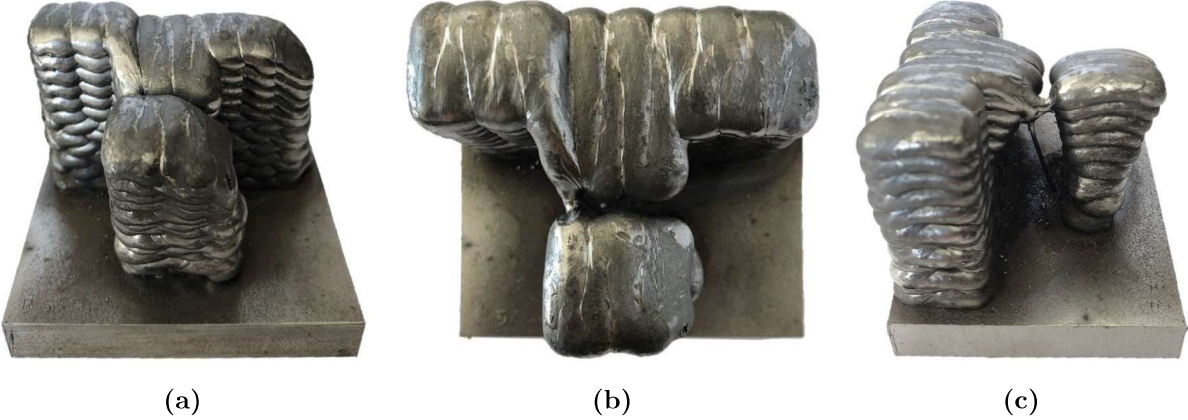


Figure 4.12: Fourth stage - Third experiment

The angle of closure of the third experiment is represented in figure 4.13.

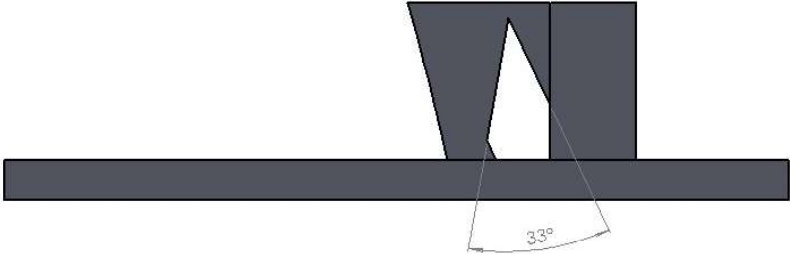


Figure 4.13: Angle of closure of third experiment

In this experiment the lozenge also did not close. However the results were better than the ones from experiment number two. In figure 4.12 - (b) and (c) is noticeable that with this gap a small closure

occurred. However the gap still is too large in order to allow a continuous deposition because in (b) it is shown that the wire kept feeding, stopping only when the substrate was hit.

Fourth Experiment

Fourth experiment is represented in figure 4.14.



Figure 4.14: Fourth stage - Fourth experiment

The angle of closure of the fourth experiment is represented in figure 4.15.

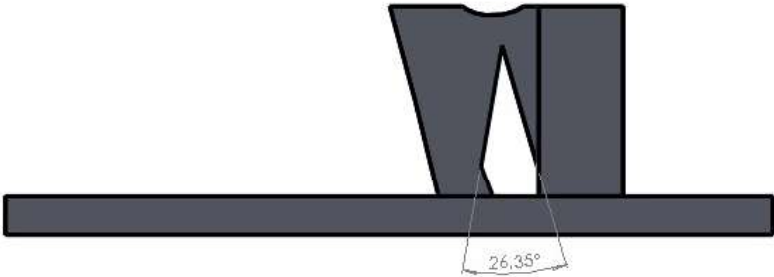


Figure 4.15: Angle of closure of fourth experiment

In this experiment the lozenge did close. However the closure was not perfect because in figure 4.14 - (b) a small tear drop metal shape is attached to the substrate. This occurs due to the feeding of the wire into the substrate at this particular position, resulting in a small deposition. However this gap was small enough to allow a continuous deposition.

Fifth Experiment

Fifth experiment is represented in figure 4.16.



Figure 4.16: Fourth Stage - Fifth experiment

The angle of closure of the fifth experiment is represented in figure 4.17.

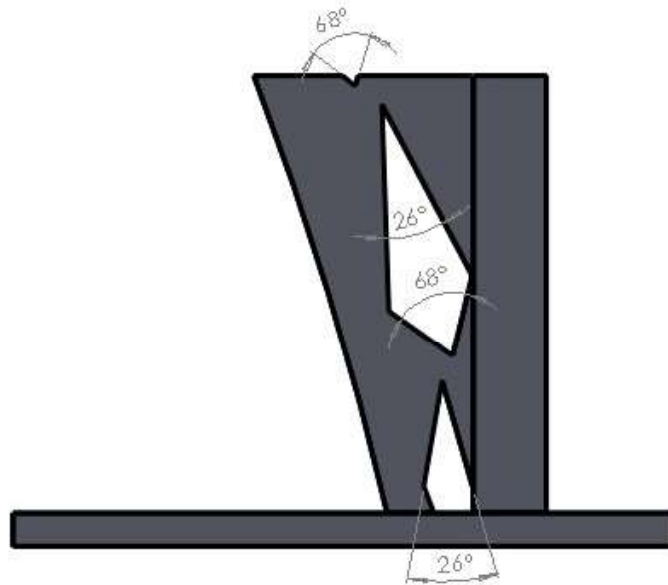


Figure 4.17: Angle of closure of fifth experiment

In this experiment the lozenge closed without any observable defects in the part deposited. This is the highest value of closure angle possible considering the parameters and conditions of the experiments performed - 26° .

4.2 Final Part

After these four stages the final part was deposited without interruptions (not considering cool-down times and closure times of the laboratory).

The parameters chosen to deposit the final part are presented in the following table 4.9.

Table 4.9: Final part parameters

Parameters	Values
Contact Tip to Work Distance [mm]	14
Shielding Gas Flow Rate [L/min]	20
Interlayer Temperature [°C]	70
Wire Feed Speed [m/min]	5.5
Travel Speed [mm/s]	5
Initial Current [A]	168
Initial Voltage [V]	11.6
Layer Height [mm]	3.5

Some images of the final part are shown in figure 4.18.

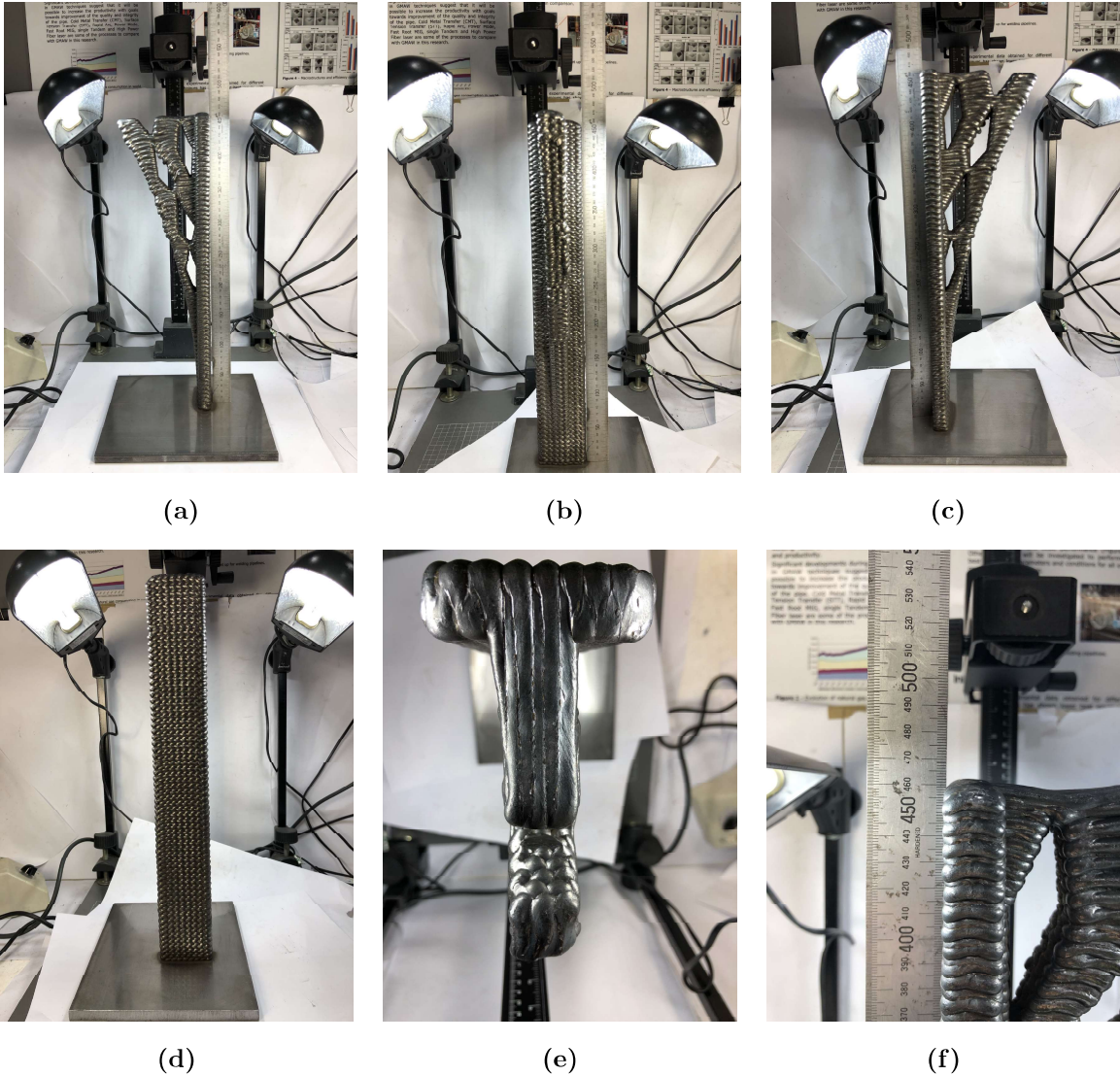


Figure 4.18: Final part

In the following table 4.10 is observed the: height of each layer, difference between each layer and the layer before, percentage of deviation between that difference and the set layer height - 3.5 mm and finally the percentage of deviation of the cumulative layer height and the cumulative set layer height. Area *A* refers to the constant base structure. On the other hand area *B* refers to the ramification region.

Regarding table 4.10 some considerations need to be highlighted:

- In order to meet the required part height, a layer height match must be performed. Thus, layers number 74, 88, 111 were deposited twice in area *A* and *B*. Layer number 118 was deposited twice only in area *B*.
- Two measuring equipments were used during the building of the final part. Until layer 43, a Digital Calliper SPI 12-527-8 (figure 3.8 - (b)) was used. The following layers were measured using a normal ruler pictured in figure 4.18 because the maximum measuring capability of the calliper was reached.

As it can be observed in table 4.10 the height of the final part is exactly the same as expected. The "% of deviation - Set layer" of the layer number 132 is 0.00%. That is excellent because means that a quasi-constant deposition was achieved (aside from four double depositions). It can also be observed that the largest values of these deviations appear in the first layers. This occurs due to the temperature of the substrate being substantially low when compared to the temperatures achieved at the time of deposition. Therefore the solidification of the molten material is faster, producing higher layer height values. Observe the following graph 4.19 in order to note the decreasing of deviation over time.

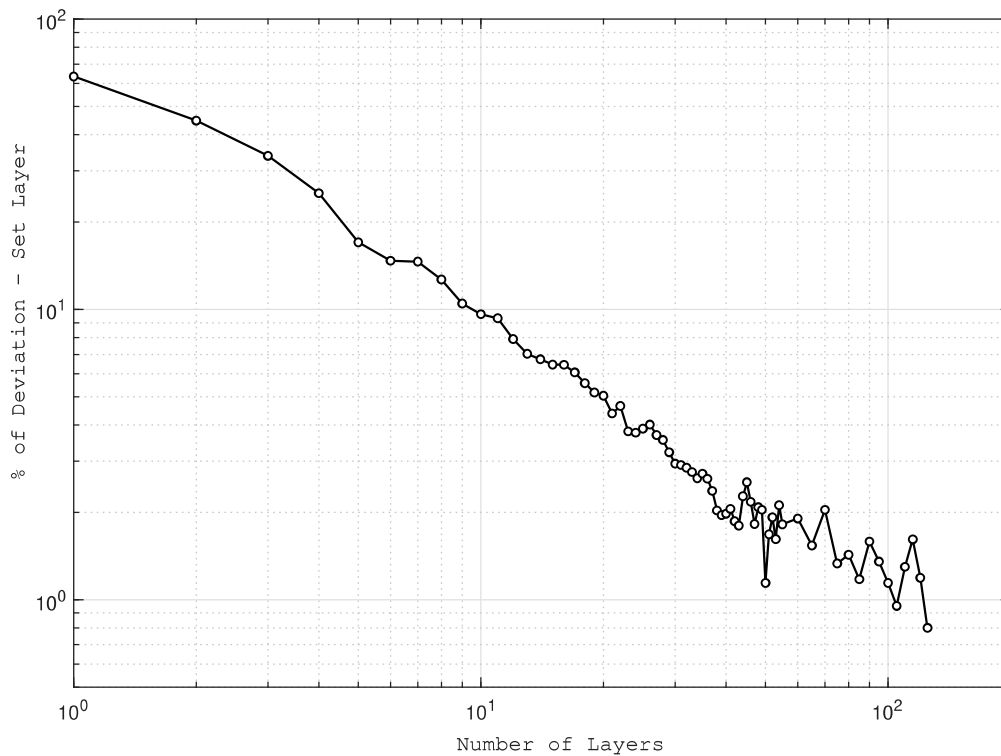


Figure 4.19: Number of Layers vs % of Deviation - Set Layer

Table 4.10: Comparison between actual layer height and expected layer height

Layer Number	A				B			
	Layer Height [mm]	Difference Between Layers [mm]	% of Deviation - Previous Layer	% of Deviation - Set Layer	Layer Height [mm]	Difference Between Layers [mm]	% of Deviation - Previous Layer	% of Deviation - Set Layer
1	5.72	-	-	63.43%	-	-	-	-
2	10.13	4.41	26.00%	44.71%	-	-	-	-
3	14.05	3.92	12.00%	33.81%	-	-	-	-
4	17.52	3.47	0.86%	25.14%	-	-	-	-
5	20.48	2.96	15.43%	17.03%	-	-	-	-
6	24.09	3.61	3.14%	14.71%	-	-	-	-
7	28.08	3.99	14.00%	14.61%	-	-	-	-
8	31.55	3.47	0.86%	12.68%	-	-	-	-
9	34.80	3.25	7.14%	10.48%	-	-	-	-
10	38.37	3.57	2.00%	9.63%	-	-	-	-
11	42.09	3.72	6.29%	9.32%	-	-	-	-
12	45.32	3.23	7.71%	7.90%	-	-	-	-
13	48.70	3.38	3.43%	7.03%	-	-	-	-
14	52.30	3.60	2.86%	6.73%	-	-	-	-
15	55.89	3.59	2.57%	6.46%	-	-	-	-
16	59.61	3.72	6.29%	6.45%	-	-	-	-
17	63.11	3.50	0.00%	6.07%	-	-	-	-
18	66.51	3.40	2.86%	5.57%	-	-	-	-
19	69.94	3.43	2.00%	5.17%	-	-	-	-
20	73.53	3.59	2.57%	5.04%	-	-	-	-
21	76.72	3.19	8.86%	4.38%	-	-	-	-
22	80.58	3.86	10.29%	4.65%	-	-	-	-
23	83.56	2.98	14.86%	3.80%	-	-	-	-
24	87.16	3.60	2.86%	3.76%	-	-	-	-
25	90.90	3.74	6.86%	3.89%	-	-	-	-
26	94.65	3.75	7.14%	4.01%	-	-	-	-
27	97.99	3.34	4.57%	3.69%	-	-	-	-
28	101.48	3.49	0.29%	3.55%	-	-	-	-
29	104.77	3.29	6.00%	3.22%	-	-	-	-
30	108.09	3.32	5.14%	2.94%	-	-	-	-
31	111.66	3.57	2.00%	2.91%	-	-	-	-
32	115.19	3.53	0.86%	2.85%	-	-	-	-
33	118.68	3.49	0.29%	2.75%	-	-	-	-
34	122.12	3.44	1.71%	2.62%	-	-	-	-
35	125.83	3.71	6.00%	2.72%	-	-	-	-
36	129.29	3.46	1.14%	2.61%	-	-	-	-
37	132.57	3.28	6.29%	2.37%	-	-	-	-
38	135.70	3.13	10.57%	2.03%	-	-	-	-
39	139.17	3.47	0.86%	1.96%	-	-	-	-
40	142.77	3.60	2.86%	1.98%	-	-	-	-
41	146.45	3.68	5.14%	2.06%	-	-	-	-
42	149.74	3.29	6.00%	1.86%	-	-	-	-
43	153.21	3.47	0.86%	1.80%	-	-	-	-
44	157.50	4.29	22.57%	2.27%	-	-	-	-
45	161.50	4.00	14.29%	2.54%	-	-	-	-
46	164.50	3.00	14.29%	2.17%	-	-	-	-
47	167.50	3.00	14.29%	1.82%	-	-	-	-
48	171.50	4.00	14.29%	2.08%	-	-	-	-
49	175.00	3.50	0.00%	2.04%	-	-	-	-
50	177.00	2.00	42.86%	1.14%	-	-	-	-
51	181.50	4.50	28.57%	1.68%	-	-	-	-
52	185.50	4.00	14.29%	1.92%	-	-	-	-
53	188.50	3.00	14.29%	1.62%	-	-	-	-
54	193.00	4.50	28.57%	2.12%	-	-	-	-
55	196.00	3.00	14.29%	1.82%	195.00	-	-	1.30%
60	214.00	18.00	2.86%	1.90%	211.00	16.00	8.57%	0.48%
65	231.00	17.00	2.86%	1.54%	229.00	18.00	2.86%	0.66%
70	250.00	19.00	8.57%	2.04%	246.00	17.00	2.86%	0.41%
75	266.00	16.00	8.57%	1.33%	264.50	18.50	5.71%	0.76%
80	284.00	18.00	2.86%	1.43%	284.00	19.50	11.43%	1.43%
85	301.00	17.00	2.86%	1.18%	300.00	16.00	8.57%	0.84%
90	320.00	19.00	8.57%	1.59%	320.00	20.00	14.29%	1.59%
95	337.00	17.00	2.86%	1.35%	334.00	14.00	20.00%	0.45%
100	354.00	17.00	2.86%	1.14%	354.00	20.00	14.29%	1.14%
105	371.00	17.00	2.86%	0.95%	370.00	16.00	8.57%	0.68%
110	390.00	19.00	8.57%	1.30%	389.00	19.00	8.57%	1.04%
115	409.00	19.00	8.57%	1.61%	408.00	19.00	8.57%	1.37%
120	425.00	16.00	8.57%	1.19%	425.00	17.00	2.86%	1.19%
125	441.00	16.00	8.57%	0.80%	441.00	16.00	8.57%	0.80%
132	462.00	21.00	14.29%	0.00%	462.00	21.00	14.29%	0.00%

In graph 4.19 both of scales are logarithmic, showing a quasi-constant slope. Therefore the deposition of the final part achieved a quasi-constant state.

During deposition some defects arose at naked eye. These are identified in the following figure 4.20.

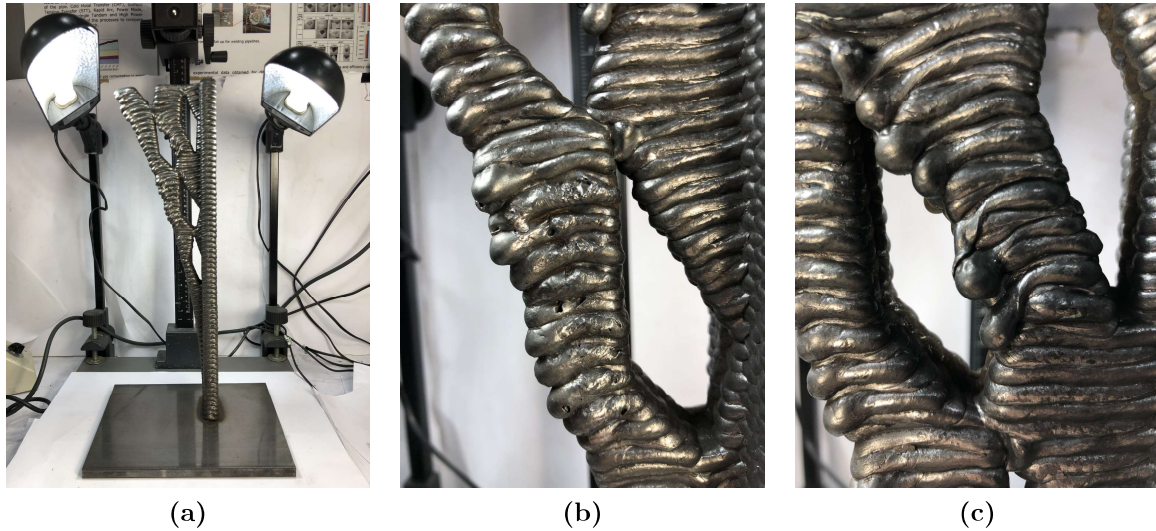


Figure 4.20: Defects of the final part

Two types of defects occurred:

- Holes in the final part (figure 4.20 - (b)) This defect arose due to a misplacement of the LEV (figure 3.4 - (d)). The latter was too close, extracting the shielding gas of the deposition area. Thus, the shielding gas was not protecting the weld pool, creating the defect. A LEV should be placed at a distance 1.5 larger than its diameter. In this case the shielding gas is a 20% CO₂ and 80% Ar, thus it is heavier than air, tending to settle in low-lying areas. Therefore the LEV should be also placed below the deposition location in order to successfully extract the gases.
- Formation of a droplet shape defect (figure 4.20 - (c)) - This defect occurred because of the low thermal gradients at the moment of deposition leading to a higher accumulation of heat than expected. This higher accumulation of heat resulted in a higher solidification time, thus creating this droplet shape defects. In this region interlayer temperature should have been lower.

4.3 Optical Macro and Microscopy Analysis

In the following subsection 4.3.1 and 4.3.2 a macroscopic and a microscopic analysis will be performed. All the samples considered are from the areas identified in figure 3.15.

4.3.1 Optical Macroscopic Observation

In the following figure 4.21 is presented the macroscopic structure of all chosen samples.

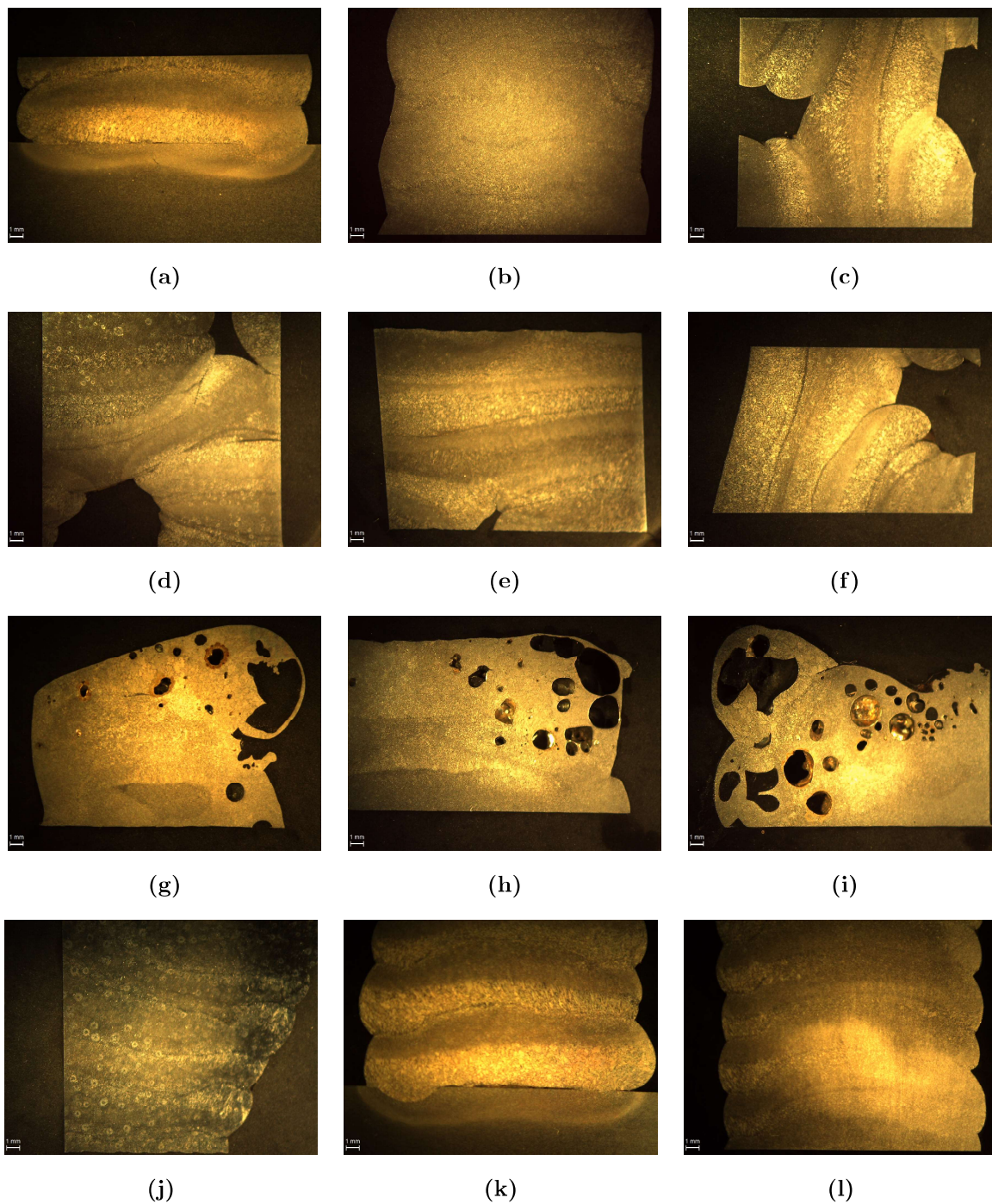


Figure 4.21: Macro-structure of the final part and of the second experiment of the third stage. (a) Substrate - Final part (b) 1 - Base (c) 2 - First intersection (d) 3 - Second intersection (e) 4 - Third intersection (f) 5 - Fourth intersection (g) 6 - Porosity region - Bottom (h) 6 - Porosity region - Middle Section (i) 6 - Porosity region - Top (j) 7 - Middle section (k) Substrate - Second experiment (l) Wall - Second experiment

In figure 4.21 are represented two sets of samples. The first ten are from the final part and the last two are from the third stage - second experiment.

As can be observed in this figure, each layer is evidenced in every single sample. Each layer includes a lighter and a darker band. According to Liberini et al. [3], there are three zones in a deposited layer. A lower zone characterized by grains of pearlitic/ferritic. This occurs due to the considerable thermal gradient that this zone suffers due to the contact with the cold substrate. Therefore ferrite grains and pearlite lamellae are formed. The second zone is the middle one and suffers the lowest thermal shock of all three. In this case the grains are pure ferrite and coarser when compared to the grains of the lower zone. This occurs due to intensity of the thermal shock being higher in the lower zone. The upper zone is the last one and suffers the largest thermal shock since it is in contact with the air that is at room temperature. The microstructure of this zone is composed of "bainite laths aggregate composed of both ferrite and cementite" and thus are of lamellar type.

In figure 4.21 - (a) and (k) is represented the deposition of a first layer. A decohesionated layer is observed in both samples. According to Prado-Cerqueira et al. [4], this decohesion results in carbides formation and oxides, thus poor surface properties are a consequence. This lack of adhesion between the first layer and the substrate occurs because the "Adjust Factor" (explained in section 3.6) was not small enough or should have been used in a more incremental way. By more incremental it means that instead of using 0.9 for the first layer and then 1 for the remaining layers, choosing for example 0.6 in the first one, 0.7 in the second, 0.9 in the third and 1 for the others. The reason behind this solution is due to the increase of heat input per length, leading to a better melt pool, thus an increase of adhesion. Also in these images can be observe a light shade band across the substrate. The latter is named Heat Affected Zone (HAZ).

Finally, in figure 4.21 - (g), (h) and (i) porosity at a big scale is observed. As explained in section 4.2, it occurred due to the close proximity of the LEV.

4.3.2 Optical Microscopic Observation

In the first two sections, samples of the third stage, second experiment will be analysed. The following ones will be from the final part.

Third Stage - Second Experiment - Substrate

In the following figure 4.22 can be observed a lack of adhesion between the first layer and the substrate as mentioned in the previous subsection 4.3.1. Also in figure 4.22 - (b), two type of grains can be observed. At the bottom, which is the substrate, and according to Stanciu et al. [34] the material "is characterized by a ferito-pearlitic microstructure with specific elongated grains" since the substrate material is delivered after suffering a process of rolling. Near the decohesionated layer, at the top, an oversized grain structures appeared.

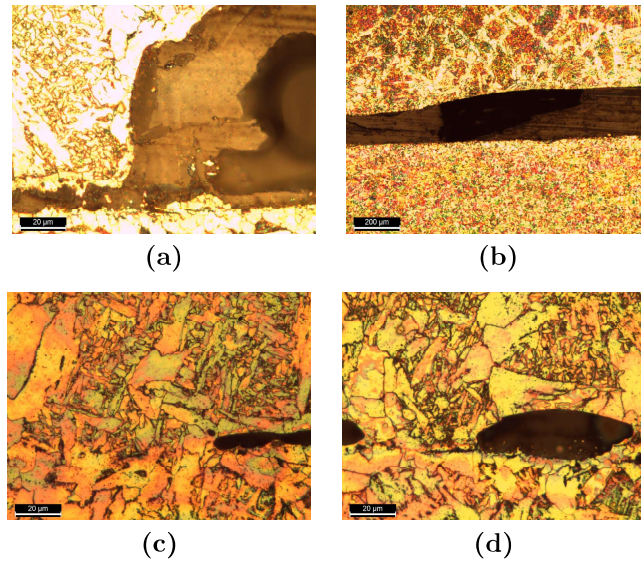


Figure 4.22: Substrate sample of third stage - Second experiment

Third Stage - Second Experiment - Wall

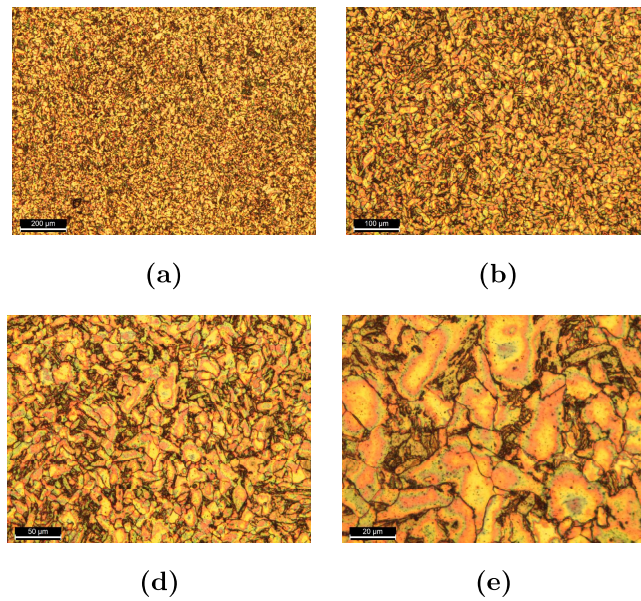


Figure 4.23: Wall sample of third stage - Second experiment

Reducing grain size increases the number of grain boundaries, therefore improving mechanical strength of an object. The latter improves because grain boundaries disrupt the motion of dislocations through a material. Since in figure 4.23 grains exhibit an expected size and the samples present no porosity, the final part is expected to have a value of UTS and YS in agreement with the values obtained when conventional methods are employed. Thus, the parameters used in this experiment were applied in the deposition of the final part.

The following subsections will only cover samples from the final part.

Substrate

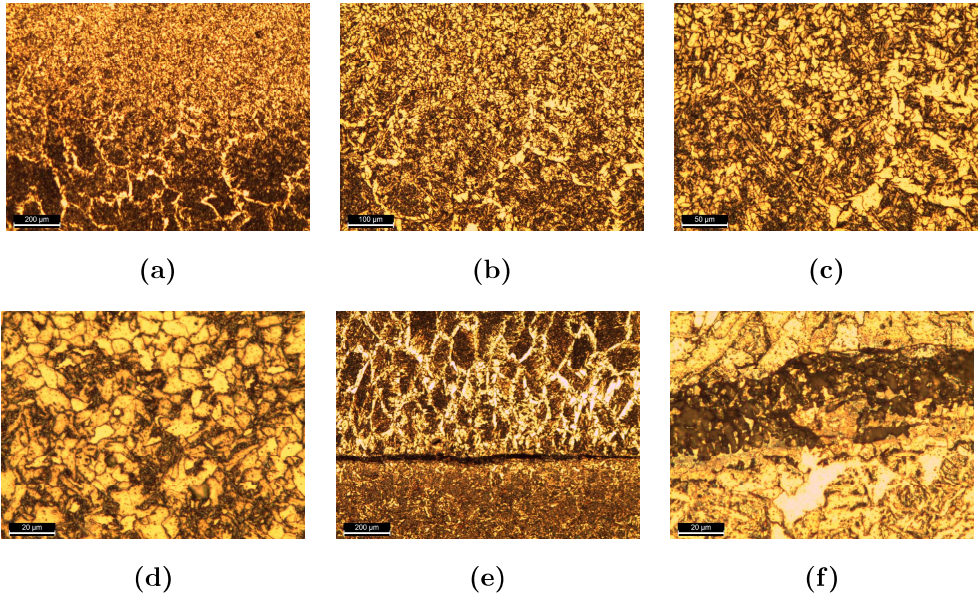


Figure 4.24: Final part sample of substrate

In figure 4.24 - (a) to (d), a lower pearlitic/ferritic zone can be observed . In figure 4.24 - (e), a lack of adhesion between the first layer and the substrate is noticeable. The explanation of this decohesionated layer is in subsection 4.3.1. Also the difference in grain size observed in figure 4.24 - (e) is discussed in this subsection.

1 - Base

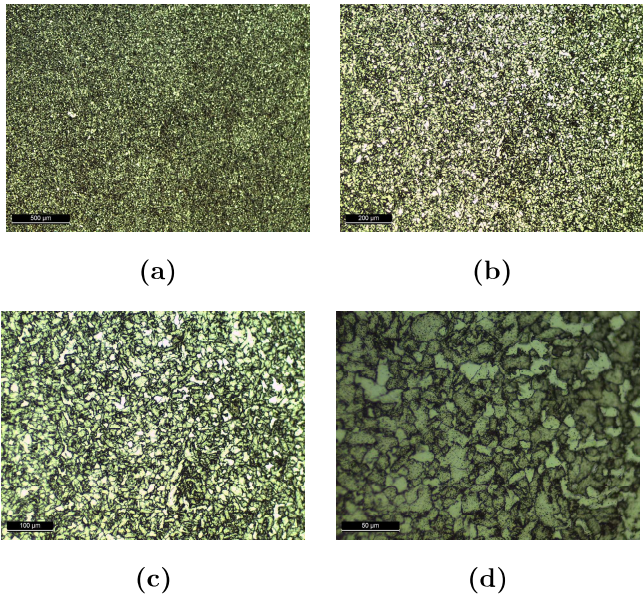


Figure 4.25: Final part sample of base

In figure 4.25 - (a) to (d), a lower pearlitic/ferritic zone can be observed. In this sample there is no sign of porosity as well as no cracks.

2 - First intersection

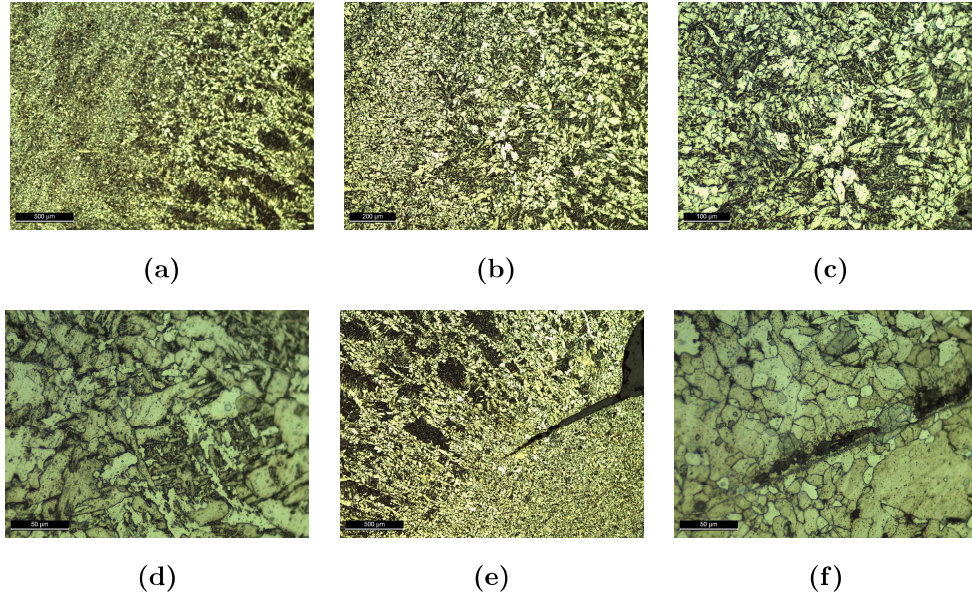


Figure 4.26: Final part sample of first intersection

In this sample there is relevant information. In figure 4.26 - (a) and (b) it can be observed a clearly transition zone between the lower zone and the middle zone as stated by Liberini et al. [3]. In 4.26 - (c) and (d) it is represented a bainitic upper zone. Finally, in figure 4.26 - (e) a solidification cracking is noticeable. According to O'Brien [35] solidification cracking is a "hot cracking defect that occurs along solidification grain boundaries (SGB) during solidification".

3 - Second intersection

In the following figure 4.27 - (a) to (c) and (d) is represented a transition zone between the lower zone and the middle zone and a pure ferritic middle zone, respectively, with no signs of porosity. In figure 4.27 - (e) to (g) a crack can be observed. However there is a possibility of being a crack that propagated in the polishing phase. This occurred because a small v-shape was already indented in the side of the final part and is known in engineering for being a stress concentration area. Thus during the polishing phase the stress was so high at this small location that the crack propagated.

4 - Third intersection

Once again in the following figure 4.28 - (a) to (e) transition zone between the lower zone and the middle zone is observed. At a first impression in figure 4.28 - (c), the small black hole seems to be porosity. However at a closer inspection (figure 4.28 - (d)), it is noticeable that it just a debris or an oxidation since the material used to build the final part is a mild steel, therefore has the tendency of rusting in a short period of time. Once more a solidification crack appears in a sample.

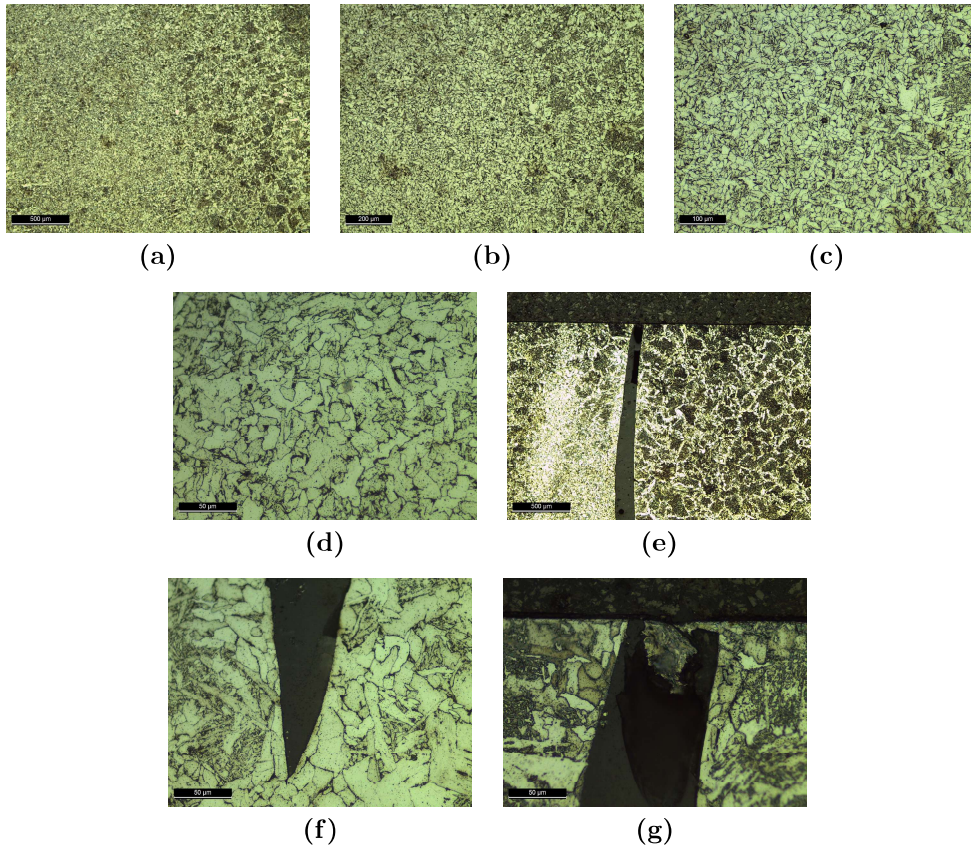


Figure 4.27: Final part sample of second intersection

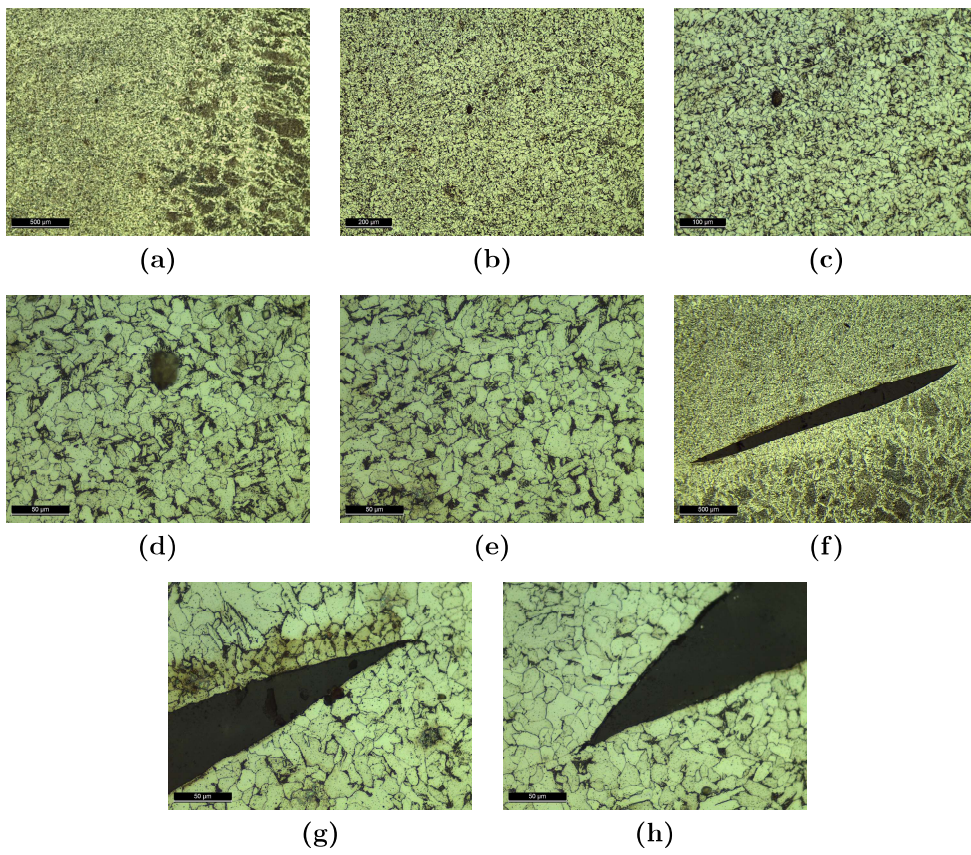


Figure 4.28: Final part sample of third intersection

5 - Fourth intersection

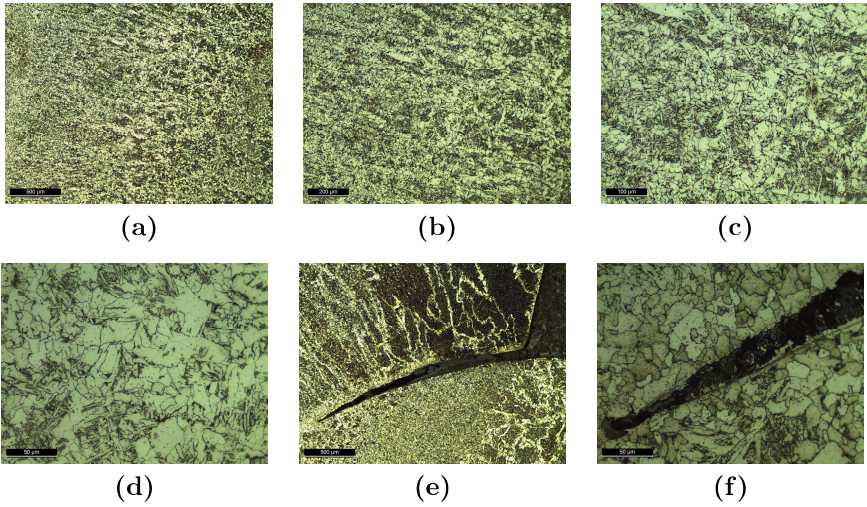


Figure 4.29: Final part sample of fourth intersection

In figure 4.29 - (a) to (d) a bainitic upper zone is represented without any signs of porosity. Once more in figure 4.29 - (e) and (f) a crack due to a stress concentration as explained in subsection 4.3.2 appears.

6 - Porosity Region

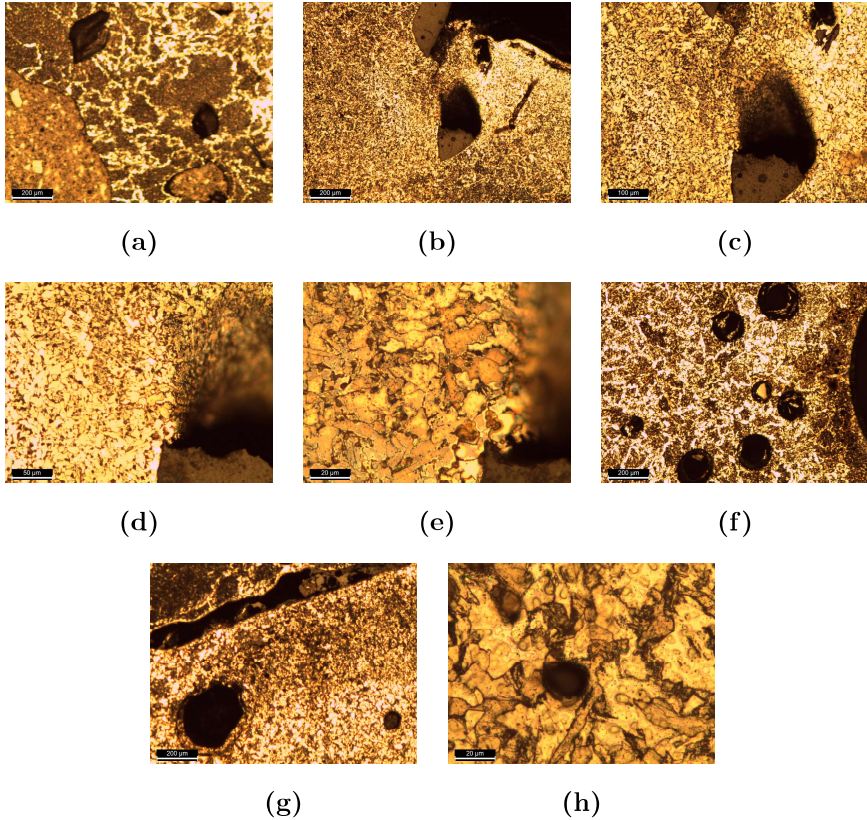


Figure 4.30: Final part sample of porosity region

In figure 4.30 a considerable amount of porosity is noticeable. This happened due to the proximity of the LEV as explained before. Thus it was not an outcome of bad parametrization but an equipment displacement malfunction.

7 - Middle Section

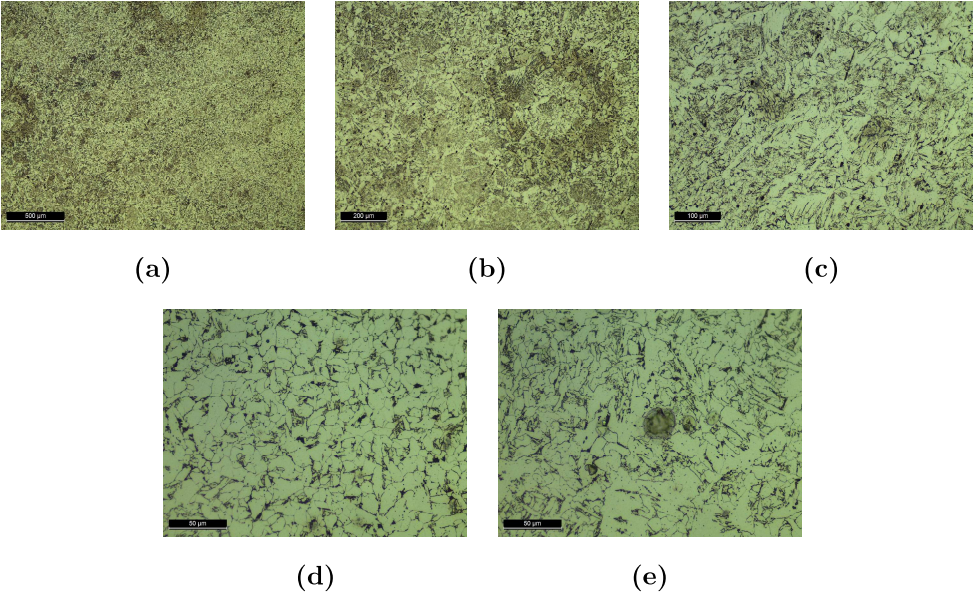


Figure 4.31: Final part sample of middle section

In figure 4.31 a bainitic upper zone is represented. There is no porosity, however an impurity can be observed in figure 4.31 - (e).

4.3.3 Conclusion Remarks

Besides the porosity region samples, porosity was not encountered. The latter is a variable of the utmost importance because reduces the mechanical strength of every material. It increases stress concentration at this location and induce internal fissures that may result in the fracture of the part. Thus this is an outstanding result in agreement with Liberini et al. [3] since porosity was expect even at a small scale.

Regarding solidification cracking, there are ways to mitigate its occurrence. According to Pires [36], control of weld metal composition, use of more favourable welding conditions and control of solidification structures are approaches to reduce the likelihood of hot cracking occurrence.

4.4 Micro Hardness

Pavlina and Van Tyne [37] achieved a correlation between Vickers Hardness and Tensile Strength with a coefficient R^2 value of 0.9347 and an error of 112 MPa. It also achieved a correlation between Vickers Hardness and Yield Strength with a coefficient R^2 value of 0.9212 and an error of 102 MPa. The correlation equations are:

$$TS = -99.8 + 3.734HV \quad (4.1)$$

$$YS = -90.7 + 2.876HV \quad (4.2)$$

In the following table 4.11 and graph 4.32 is shown the collected data of the Vickers Hardness and its correlation with the Ultimate Tensile Strength and Yield Strength for the samples analysed.

Table 4.11: Correlation of Vickers Hardness with Ultimate Tensile Strength and Yield Strength

Variables	Samples											
	A	B	C	D	E	F	G	H	I	J	K	L
Vickers Hardness [HV]	140	166	179	203	182	175	174	179	181	173	179	175
	167	173	185	204	193	176	182	182	182	175	180	176
	177	175	196	205	199	184	184	194	185	175	184	177
	184	175	214	206	201	185	186	194	190	176	194	180
	186	175	216	207	202	188	197	196	192	177	197	181
	186	179	217	208	203	193	199	196	196	179	202	184
	188	180	217	208	203	196	202	200	197	181	212	186
	193	181	220	208	206	197	205	200	205	190	217	186
	193	186	226	227	212	202	208	201	209	192	219	192
	193	190	227	228	214	219	211	203	211	202	219	194
Average Vickers Hardness [HV]	180.70	178.00	209.70	210.40	201.50	191.50	194.80	194.50	194.80	182.00	200.30	183.10
Ultimate Tensile Strength [MPa]	775.62	765.52	884.08	886.70	853.41	816.01	828.35	827.23	828.35	780.48	848.92	784.59
Average Ultimate Tensile Strength [MPa]	823.27											
Yield Strength [MPa]	428.99	421.23	512.40	514.41	488.81	460.05	469.54	468.68	469.54	432.73	485.36	435.90
Average Yield Strength [MPa]	465.64											

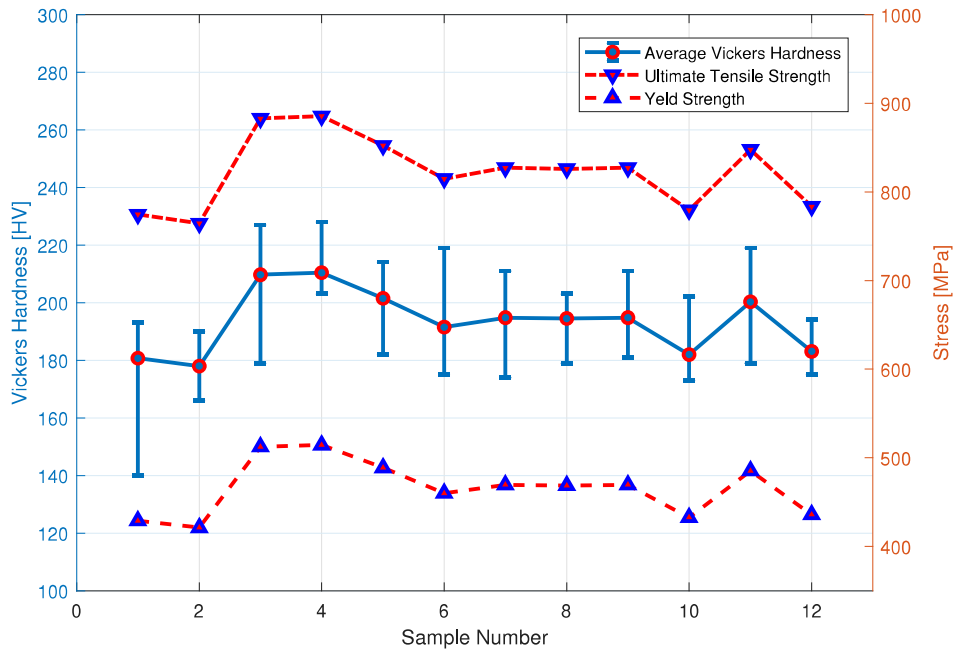


Figure 4.32: Correlation of Vickers Hardness with Ultimate Tensile Strength and Yield Strength

With respect to table 4.11 and 4.32, the average final part Ultimate Tensile Strength is 822.11 *MPa* and Yield Strength is 465.64 *MPa*. These values are in agreement with the ones stated by Cranfield University for mild steel [38]. UTS value is around 750 *MPa* and YS value is around 500 *MPa*.

4.5 Path Efficiency

Calculation of the path efficiency will be performed regarding only the deposition of the final part.

Path efficiency (PE) is the ratio between the Arc-On Time (Arc-OT) and the Total Time (TT). The Total Time is the total duration of deposition of a certain layer.

$$PE = \frac{Arc - OT}{TT} \quad (4.3)$$

The following table 4.12 and figure 4.33 presents the various times in order to calculate path efficiency.

Table 4.12: Duration of deposition and path efficiency

Layers Number	Duration of Deposition [h:m:s]	Arc-On Time [h:m:s]	Arc-Off Time [h:m:s]	Path Efficiency [%]
1	00:01:39	00:01:39	00:00:00	100.00%
10	00:01:01	00:01:01	00:00:00	100.00%
20	00:01:02	00:01:02	00:00:00	100.00%
30	00:01:05	00:01:05	00:00:00	100.00%
40	00:01:10	00:01:10	00:00:00	100.00%
50	00:01:16	00:01:16	00:00:00	100.00%
60	00:01:26	00:01:13	00:00:13	85.18%
70	00:01:31	00:01:21	00:00:10	89.13%
80	00:01:40	00:01:27	00:00:12	87.45%
90	00:01:43	00:01:34	00:00:09	90.94%
100	00:02:08	00:02:08	00:00:00	100.00%
110	00:02:09	00:01:53	00:00:16	87.59%
120	00:02:26	00:02:10	00:00:16	89.04%
130	00:02:40	00:02:31	00:00:09	94.13%

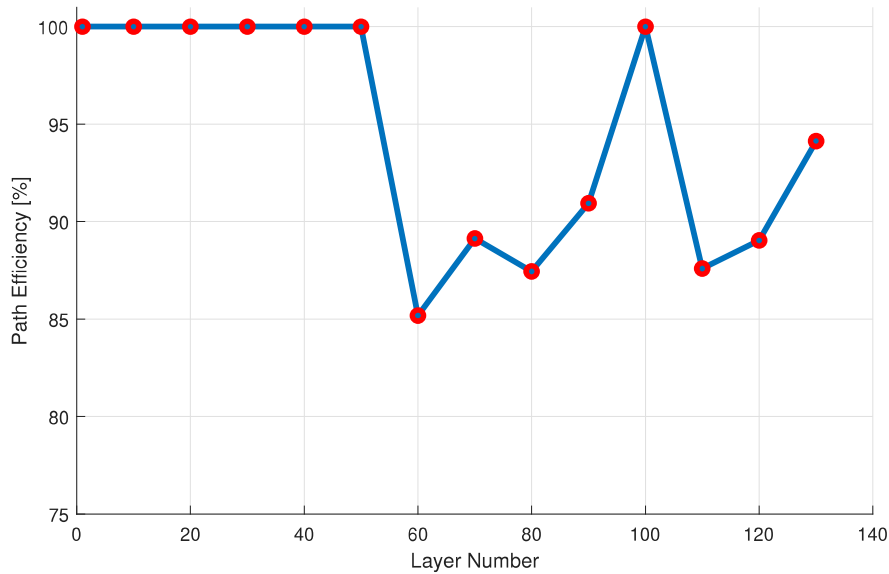


Figure 4.33: Path efficiency

As it can be observed in figure 4.12 and in table 4.33, the first 50 layers have a path efficiency of 100.00%. The path of deposition of these layers is continuous, hence this percentage. When the percentage is not 100.00%, the reason behind it is because the path of deposition is not continuous. It happens when the ramification part starts. In this case the Arc-Off Time is due to the motion of the robot to the home position and back to the next deposition position. Thus, the path efficiency can be increased, decreasing the length of this motion.

4.6 Substrate Deformation

The substrate deformation was only taken into account in the deposition of the final part as in the chapter 4.5. This occurred because the experiments were performed with the aim of using each substrate as much as possible as pictured in the following figure 4.34.



Figure 4.34: Substrate usage during experiments

Substrate deformation was 1.25 mm . This type of distortions arise because of the residual stresses. In this case it was small because the heat is only conducted from the part to the substrate through a small area of the base of the final part. This fact is supported by Williams et al. [14] which states that "the deposition of shorter layers leads to lower residual stress and distortion".

The path of deposition as well as the clamping systems play a fundamental role in order to mitigate these type of distortions.

Chapter 5

Conclusions

5.1 Achievements

The part to be achieved was studied and improved throughout this work with the use of a CAD software, a WAAM software and a significant number of set-ups and equipments.

The study started by choosing a specific representative region of the part to be achieved and modelling it in a CAD software. Then, a parametrization study was performed for the smallest and the largest dimensions of the representative part. At this point, it was concluded that the smallest dimensions showed that these dimensions were not small enough to produce defects with respect to the heat accumulation at the time of deposition. The parameters achieved for the largest dimension of the part produced good depositions. The next step was to fine tune the parameters obtained through previous experiments. After choosing the best parameters of the samples, a micro and macrostructure analysis was performed. It was concluded that the deposited sample with such parameters produced sound results. Afterwards, some experiments were performed in order to study the intersections. The main variable in this case was the degree of closure and the maximum value obtained was 26° . Finally, the representative part was deposited and analysed.

Important remarks need to be highlighted:

- A large amount of heat accumulation occurs during deposition, resulting in defects such as the ones represented in 4.20 - (b).
- Deposition of the final part was stationary with respect to the parameters employed
- The microstructure and macrostructure were in agreement with the literature. However small defects arose. There were solidification cracks as well as cracks derived from the polishing stage. These cracks only occurred in the intersections region.
- Some porosity also appeared, however it was because of a displacement malfunction of a LEV
- The deposited part and the fourth stage experiments were almost exactly identical to the CAD model when employing the best parameters achieved. Thus, WAAM is already able to guarantee a final part that requires a minimal machining stage

- As aforementioned, the maximum closure angle achieved was 26°
- An oscillation type of deposition was employed
- The final part UTS and YS are in agreement with the expected values for mild steel

Finally, the main achievement of this work is the fact that a free form deposition was performed with great results and in agreement with the ones that are obtained when using conventional methods. This is a novelty for WAAM since this feature has never been accomplished before as well as analysed to this extend. Thus, this work can be a great starting point to achieve free form structures with ease and with a guaranteed quality in the near future.

5.2 Future Work

As stated in the literature, WAAM still needs continuous research in order to improve as a solid process to replace the conventional methods. Thus, there is a possibility of a future work with the following suggestions:

- Employing a more efficient heat dissipation method than manual compressed air. Air knives would be a good compromise between cost and efficiency
- Applying SEM so to investigate the microstructure in more detail
- Replicate the analysis performed to the final part to have a larger statistical sample
- Pre-heating the substrate beforehand in order to not obtain large layer heights in the first layers.
- Applying a new process to a WAAM deposited part named shot peening in order to try to reduce residual stresses as well as improving mechanical strength
- Further research needs to be conducted regarding intersections such as the ones analysed in this work
- Finally, build the required part. However a new type of set-up needs to be assembled so that a 5m tall component is feasible

Bibliography

- [1] B. Cong, Z. Qi, B. Qi, H. Sun, G. Zhao, and J. Ding. A Comparative Study of Additively Manufactured Thin Wall and Block Structure with Al-6 . 3 % Cu Alloy Using Cold Metal Transfer Process. *Applied Sciences*, 7(275):1–11, 2017.
- [2] J. M. M. Gou. *True freeform fabrication for wire + arc additive manufacture*. Msc thesis, Cranfield University, 2017.
- [3] M. Liberini, A. Astarita, G. Campatelli, A. Scippa, G. Venturini, M. Durante, L. Boccarusso, F. Memola, C. Minutolo, and A. Squillace. Selection of optimal process parameters for wire arc additive manufacturing. *Procedia CIRP*, 62:470–474, 2017.
- [4] J. L. Prado-Cerqueira, A. M. Camacho, J. L. Diéguez, Á. Rodríguez-Prieto, A. M. Aragón, C. Lorenzo-Martín, and Á. Yanguas-Gil. Analysis of favorable process conditions for the manufacturing of thin-wall pieces of mild steel obtained by wire and arc additive manufacturing (WAAM). *Materials*, 11(1449):1–18, 2018.
- [5] A. Busachi, J. Erkoyuncu, P. Colegrove, F. Martina, and J. Ding. Designing a WAAM based manufacturing system for defence applications. *Procedia CIRP*, 37(2013):48–53, 2015.
- [6] W. E. Frazier. Metal additive manufacturing: A review. *Journal of Materials Engineering and Performance*, 23(6):1917–1928, 2014.
- [7] ISO/TC 261. ISO/ASTM 52900:2015: Additive manufacturing-General principles-Terminology. 12, 2015.
- [8] G. N. Levy, R. Schindel, and J. P. Kruth. Rapid manufacturing and rapid tooling with layer manufacturing (LM) technologies , state of the art and future.
- [9] R. Kleer, C. Weller, R. Kleer, and F. T. Piller. Economic implications of 3D printing : Market structure models in light of additive manufacturing revisited. *Intern. Journal of Production Economics*, 164(October 2015):43–56, 2014.
- [10] F. Martina and S. W. Williams. Wire+arc additive manufacturing vs. traditional machining from solid: a cost comparison. Technical report, Cranfield University, Cranfield, Bedfordshire, United Kingdom, 2015.

- [11] D. Ding, Z. Pan, D. Cuiuri, and H. Li. Wire-feed additive manufacturing of metal components : technologies , developments and future interests. *The International Journal of Advanced Manufacturing Technology*, 81:465–481, 2015.
- [12] L. M. S. C. Neto. *Studying the Application of Additive Manufacturing to Large Parts*. Extended abstract, Instituto Superior Técnico, 2017.
- [13] Baker Ralph. United States Patent Office, 1925.
- [14] S. W. Williams, F. Martina, A. C. Addison, J. Ding, G. Pardal, and P. Colegrove. Wire + Arc Additive Manufacturing. *Materials Science and Technology*, 32(7):641–647, 2015.
- [15] J. Pandremenos, C. Doukas, P. Stavropoulos, and G. Chryssolouris. Machining with robots: a critical review. In *7th International Conference on Digital Enterprise Technology*, number September, pages 1–8, Athens, 2011.
- [16] J. Ding, P. Colegrove, J. Mehnen, S. Ganguly, P. M. Almeida, F. Wang, and S. Williams. Thermo-mechanical analysis of Wire and Arc Additive Layer Manufacturing process on large multi-layer parts. *Computational Materials Science*, 50(12):3315–3322, 2011.
- [17] M. I. Castro e Silva. *Study of deposition strategies of a wire + arc additive manufactured component*. Msc thesis, 2018.
- [18] I. d. F. P. A. Pires. *Joining Processes - Gas Tungsten Arc Wleding (GTAW)*. Instituto Superior Técnico, Lisbon, 2017.
- [19] M. I. Khan. *Welding Science and Technology*. New Age International, 2007.
- [20] F. Wang, S. Williams, P. Colegrove, and A. A. Antonysamy. Microstructure and mechanical properties of wire and arc additive manufactured Ti-6Al-4V. *Metallurgical and Materials Transactions A: Physical Metallurgy and Materials Science*, 44(2):968–977, 2013.
- [21] I. d. F. P. A. Pires. *Joining Processes - Plasma Arc Welding (PAW)*. Instituto Superior Técnico, Lisbon, 2017.
- [22] F. Martina, J. Mehnen, S. W. Williams, P. Colegrove, and F. Wang. Investigation of the benefits of plasma deposition for the additive layer manufacture of Ti-6Al-4V. *Journal of Materials Processing Technology*, 212(6):1377–1386, 2012.
- [23] I. d. F. P. A. Pires. *Joining Processes - Gas Metal Arc Wleding (GMAW)*. Instituto Superior Técnico, Lisbon, 2017.
- [24] V. R. Duarte. *Additive manufacturing of a high resistance steel by MIG / MAG*. Msc thesis, Universidade Nova de Lisboa, 2016.
- [25] Fronius. CMT Advanced: A higher deposition rate, better gap-bridging ability and higher stability, 2019.

- [26] S. Selvi, A. Vishvaksean, and E. Rajasekar. Cold metal transfer (CMT) technology - An overview. *Defence Technology*, 14(1):28–44, feb 2018.
- [27] K. Furukawa. New CMT arc welding process – welding of steel to aluminium dissimilar metals and welding of super-thin aluminium sheets. *Welding International*, 20(6):440–445, 2006.
- [28] C. G. Pickin and K. Young. Evaluation of cold metal transfer (CMT) process for welding aluminium alloy. *Science and Technology of Welding and Joining*, 11(5):583–585, 2006.
- [29] Weldwire Company Inc. .Thecnical Information: Steel Wires Bare - ER70S-6.
- [30] S. Davidson. Grasshopper - Algorithmic Modeling for Rhino, 2015. URL <https://www.grasshopper3d.com/>.
- [31] R. & A. McNeel. Rhino 6 Features, 2018. URL <https://www.rhino3d.com/6/features>.
- [32] Nikon Optishot microscope. URL <https://www.spachoptics.com/NIKON-OPTIPHOT-DIC-p/nikon-optiphot-dic.htm>.
- [33] Schott KL 1500 electronic. URL <https://labstuff.eu/en/schott-kl-1500-electronic.html>.
- [34] E. M. Stanciu, A. Pascu, and I. Gheorghiu. CMT Welding of Low Carbon Steel Thin Sheets. *IOP Conference Series: Materials Science and Engineering*, 209(1):1–8, 2017.
- [35] E. D. O’Brien. *Welding with low alloy steel filler metal of X65 pipes internally clad with Alloy 625: application in pre-salt oil extraction*. Msc thesis, The Ohio State University, 2016.
- [36] I. d. F. P. A. Pires. *Joining Processes - Weldability problems*. Instituto Superior Técnico, Lisbon, 2017.
- [37] E. J. Pavlina and C. J. Van Tyne. Correlation of Yield strength and Tensile strength with hardness for steels. *Journal of Materials Engineering and Performance*, 17(6):888–893, 2008.
- [38] *WAAM - Mechanical properties*. Cranfield University, November, 2017.

Appendix A

Technical Data Sheets

SupraMigUltra®






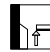
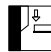
CLASSIFICATION									
AWSA5.18	ER70S-6	A-Nr	1	Mat-Nr	1510				
EN ISO 14341-A	G46 3C4S1/G50 5M4S1	F-Nr	6						
		9606FM	1						
GENERAL DESCRIPTION									
Solid wire with increased manganese for semi-automatic welding and robotic applications									
Excellent feedability and very consistent welding performance									
Tight and stable arc with extremely low spatter									
Also provided in Accutrak® drum									
WELDING POSITIONS (ISO/ASME)					SHIELDING GASES (ACC. ISO 14175)				
							M21	Mixed gas Ar+>15-25% CO ₂	
						Cl	Active gas 100% CO ₂		
APPROVALS									
ABS	BV	DNV/GL	RINA	LRS	DB	TÜV	CE	QWB	
+	+	+	+	+	+	+	+	+	
CHEMICAL COMPOSITION (W%) TYPICAL WIRE									
C	Mn	Si							
0,08	1,70	0,85							
MECHANICAL PROPERTIES, TYPICAL, ALL WELD METAL									
		Shielding gas	Condition	Yield strength (N/mm ²)	Tensile strength (N/mm ²)	Elongation (%)	Impact ISO-V(0)		
Typical values		M21	AW	500	650	26	-20°C	-40°C	-50°C
		Cl	AW	490	620	30	80	80	70
							60	50	
EXAMPLES OF MATERIALS TO BE WELDED									
Steel grades	Standard	Type							
General structural steels	EN 10025	S185, S235, S275, S355							
Ship plates	ASTM A131	Grade A, B, D, AH32 to DH36							
Cast steels	EN 10219-2	GP240R							
Pipe material	EN 10208-1	L210, L240, L290, L360							
	EN 10208-2	L240NB, L290NB, L360NB, L360QB, L240MB, L290MB, L360MB, L415MB, L415NB							
	API 5LX	X42, X46, X52, X60							
	EN 10216-1	P235T1, P235T2, P275T1							
	EN 10217-1	P275T2, P355N							
Boiler & pressure vessel steels	EN 10028-2	P235GH, P265GH, P295GH, P355GH							
Fine grained steels	EN 10025 part 3	S275, S355, S420, S460							
	EN 10025 part 4	S275M, S275ML, S355M, S355ML, S420M, S420ML, S460, P460, S460ML							
PACKAGING AND AVAILABLE SIZES									
Diameter (mm)	0,8	1,0	1,2	1,4	1,6				
16 kg spool B300	X	X	X	X	X				
16 kg spool B5300		X	X						
15 kg spool S300		X	X						
250 kg Accutrak® Drum		X	X	X					
500 kg Accutrak® Drum		X	X	X					

Figure A.1: Deposited material data sheet

Appendix B

Software Files

B.1 Builddata File

```
<?xml version="1.0" encoding="utf-8"?>
<BuildParts>
  <section>
    <Guid>2c0253fa-5d57-4bd8-ae9e-3128aefbcd15</Guid>
    <SecNum>1</SecNum>
    <ShaNuM>2</ShaNuM>
  </section>
  <section>
    <Guid>14db0025-8874-4473-bbfe-34daa7d148b3</Guid>
    <SecNum>2</SecNum>
    <ShaNuM>2</ShaNuM>
  </section>
  <section>
    <Guid>1a757f82-d938-4bb9-b5ab-361542930dcd</Guid>
    <SecNum>3</SecNum>
    <ShaNuM>2</ShaNuM>
  </section>
  <section>
    <Guid>c65ad248-efc7-480e-a530-5f5a77bd9c67</Guid>
    <SecNum>4</SecNum>
    <ShaNuM>2</ShaNuM>
  </section>
  <section>
    <Guid>8b916875-ba8c-418d-bb77-bf3ae0530bd3</Guid>
    <SecNum>5</SecNum>
    <ShaNuM>2</ShaNuM>
  </section>
</BuildParts>
```

Figure B.1: Builddata example file

B.2 ABB Programme File

```
Cmtready;
Cmtoff;
MoveJ ahome,v150,fine,cmtdemo\WObj:=abbright;
SetGo goJOB.1;
Move_X:= 0;
Move_Y:=0;
Move_Z:=0;
MoveL Offs(astart,Move_X,Move_Y,Move_Z),v80,fine,cmtdemo\WObj:=abbright;
WaitTime 5;
Cmton;
WaitTime 1.2;
WHILE Move_X<=116
    • Move_Y:=20;
    • MoveL Offs(astart,Move_X,Move_Y,Move_Z),TS,fine,cmtdemo\WObj:=abbright;
    • Move_X:=Move_X+4;
    • MoveL Offs(astart,Move_X,Move_Y,Move_Z),TS,fine,cmtdemo\WObj:=abbright;
    • Move_Y:=0;
    • MoveL Offs(astart,Move_X,Move_Y,Move_Z),TS,fine,cmtdemo\WObj:=abbright;
    • Move_X:=Move_X+4;
    • MoveL Offs(astart,Move_X,Move_Y,Move_Z),TS,fine,cmtdemo\WObj:=abbright;
ENDWHILE
Move_Y:=20;
MoveL Offs(astart,Move_X,Move_Y,Move_Z),TS,fine,cmtdemo\WObj:=abbright;
Move_X:=Move_X+4;
MoveL Offs(astart,Move_X,Move_Y,Move_Z),TS,fine,cmtdemo\WObj:=abbright;
Move_Y:=0;
MoveL Offs(astart,Move_X,Move_Y,Move_Z),TS,fine,cmtdemo\WObj:=abbright;
Cmtoff;
WaitTime 3;
MoveJ ahome,v150,fine,cmtdemo\WObj:=abbright;
Stop
MoveL astart,v80,fine,cmtdemo\WObj:=abbright;
```

Figure B.2: ABB programme example file

